Tissue-specific adaptation of human T cells is preserved during tissue inflammation

Nicole B. Potchen[1], Hugh R. MacMillan[1], Eva Domenjo-Vila[1], Andrew J. Konecny[1,2], Alexis K. Taber[1], Caitlin S. DeJong[1], Geervani Daggupati[1,2], Raj Shree[3], Stephen A. McCartney[3], Shelton W. Wright[4], Evan W. Newell[1,6], Douglas R. Dixon[5], Martin Prlic[1,6*]

[1] Vaccine and Infectious Disease Division, Fred Hutchinson Cancer Center, Seattle, WA, USA.

[2] Department of Immunology, University of Washington, Seattle, WA, USA.

[3] Division of Maternal Fetal Medicine, Department of Obstetrics and Gynecology, University of Washington, Seattle, WA, USA.

[4] Division of Pediatric Critical Care Medicine, Department of Pediatrics, University of Washington, Seattle, WA, USA.

[5] Department of Bioscience Research and Periodontics, University of Tennessee Health Science Center, College of Dentistry, Memphis, TN, USA.

[6] Department of Global Health, University of Washington, Seattle, WA, USA.

* Corresponding author

Fred Hutchinson Cancer Center, Vaccine and Infectious Disease Division, Seattle, WA, USA.

mprlic@fredhutch.org

Summary

T cells play an essential role in protecting tissues against pathogens and regulating tissue homeostasis. Previous studies highlight that T cells display tissue-specific phenotypic and functional properties, suggesting that T cells adapt to their local environment. However, whether this holds true in inflamed tissues or whether inflammation disrupts any tissue-specific T cell adaptations remains poorly understood. To address this open question, we examined the T cell compartment – including conventional CD4 and CD8 T cells, regulatory T cells, γδ T cells, and MAIT cells – from healthy and inflamed human mucosal tissues. Using high-parameter spectral flow cytometry, we examined phenotype *ex vivo* and the functional capacity following stimulation, utilizing conventional gating and unsupervised clustering analysis approaches. Overall, we analyzed 65 tissue samples including mild, moderate, and severely inflamed oral gingiva, healthy and inflamed lung, along with healthy and inflamed tissue from the decidual-placental interface. Across these mucosal barrier tissues, we find that tissue location plays a dominant role in shaping the composition, phenotype, and functional capacity of the T cell compartment. Importantly, these tissue-specific adaptations were largely maintained during states of tissue inflammation. This included the ability to exert tissue repair functions, which was preserved across T cell subsets, even in severely inflamed tissues.

Introduction

Human T cells have distinct phenotypic and functional properties across different tissues and organs. This was initially demonstrated by Farber and colleagues who examined the phenotype and functional properties of conventional CD4 and CD8 T cells isolated from secondary lymphoid tissues, lung, jejunum, ileum and colon of trauma-induced, deceased organ donors[1]. This study furthermore established CD69 expression as biomarkers for tissue-residence for human CD4 T cells, and CD69 and CD103 co-expression to indicate tissue-resident CD8 T cells[1]. Follow-up studies highlighted that expression of CD69 by human CD4 and CD8 T cells is associated with a core transcriptional signature akin to bona fide murine tissue-resident T cells[2]. Human tissue-resident memory CD8 T cells (T_{RM}) show tissue-specific adaptation such as distinct cytotoxic properties across skin, lung, and jejunum, and are also clonally distinct across these tissue sites[3-7]. A recent study indicated that within the intestine, distinct tissue niches drive unique phenotypic and functional properties in T cells, thus providing further compelling evidence that T_{RM} tissue location and functional state are fundamentally linked[8].

Similarly, conventional CD4 T cells (CD4 Tconv) and regulatory T cells (CD4 Treg) also have distinct phenotypic and functional properties across tissues[9-12]. Further evidence points to innate-like T cells also adapting in a tissue-specific manner. Human $\gamma\delta$ T cells differ by tissue location with cells from adult lung, spleen, lymph nodes (LNs), and gut tissue clustering differentially by tissue based on their expression of transcripts associated with effector and repair functions[13]. Human mucosal-associated invariant T (MAIT) cells in tissues have distinct T cell receptor (TCR) repertoires, cytokine expression profiles, and display a more activated phenotype compared to counterparts in the blood[14,15].

Whether tissue-specific adaptations are maintained during tissue inflammation is unclear. Inflammation involves coordinated immune cell recruitment and activation and thus has the potential to profoundly alter the T cell compartment within tissue[16]. Memory phenotype CD8 T

63 cells can be activated by pro-inflammatory signals alone; this event has been coined bystander-
64 activation or inflammation-driven activation of T cells[17,18]. Inflammation-driven activation of
65 memory CD8 T cells leads to increased expression of CD69, PD-1, and TOX, along with
66 expression of IFNγ and Granzyme B (GzmB)[19-23] which can have protective properties[24,25] but can
67 also lead to tissue pathologies[26]. Such bystander-activated CD8 T cell-mediated pathology has
68 been demonstrated in a human cohort following infection with Hepatitis A virus (HAV)[27]. For CD4
69 T cells, inflammation and associated tissue pathology is often associated with expression of IL-
70 17, but it is noteworthy that IL-17 should not be simply viewed as a pro-inflammatory cytokine[28]
71 or indicator of excessive inflammation[29]. Importantly, in addition to mediating tissue protection and
72 pathology, T cells also play a role in restoring tissue homeostasis via secretion of IL-22 and the
73 epidermal growth factor receptor (EGFR)-ligand amphiregulin (AREG)[30-32]. Tregs express AREG
74 in response to IL-18 and IL-33[33], while a recent study demonstrates that human memory CD8 T
75 cells express AREG in response to TCR stimulation[34].

76 While there has been substantial progress in our understanding of the T cell compartment
77 and its tissue-specific functional properties in healthy human tissues, the extent to which
78 inflammation alters these functional properties remains an open question. We sought to address
79 if inflammation overrides any tissue-specific T cell adaption in human tissues. Specifically, we
80 aimed to determine if inflammation alters the composition of the T cell compartment and
81 associated functional properties, and if it affects the ability of T cells to maintain their tissue-
82 regenerative functions. To accomplish this, we collected healthy and inflamed tissues from 3
83 distinct mucosal barrier sites: oral mucosa (gingiva), lung, and the decidual-placental interface
84 (DPI). We developed a high-parameter flow cytometry panel containing 37 markers to define the
85 composition, phenotype, and functional capacity of the T cell compartment: CD4 Tconv, CD4
86 Treg, CD8 CD103+ T_{RM} and CD8 CD103- circulating T cells, along with the innate-like MAIT and
87 γδ T cell subsets. Overall, we found that the composition, phenotype and function of the T cell

88 compartment was driven more by tissue location than inflammation, indicating that T cells largely
89 maintain their tissue-specific adaptations during inflammation. Our data emphasize the need to
90 assess and consider inflammation in a tissue-specific manner. Furthermore, our data highlight
91 that T cells maintain their tissue-regenerative capacity even in severely inflamed tissues, thus
92 pinpointing T cells as a therapeutic target to treat inflammatory diseases.

93 # Results

94 **The inflammation state in the oral mucosa has a moderate effect on composition and**
95 **phenotype of the T cell compartment**

96 To determine the impact of inflammation on the mucosal T cell compartment, we first
97 examined phenotypic differences across mildly, moderately, and severely inflamed gingival
98 tissues. These tissues are discarded from routine surgeries and represent a wide range of
99 inflammatory states. We assigned clinically healthy gingival tissue and tissue with mild gingivitis
100 as "mild inflammation" since even clinically healthy tissue contains a baseline level of
101 inflammation, which may allow for constant immune surveillance[35]. Next, we assigned tissues
102 with pronounced gingivitis transitioning to periodontitis as "moderate inflammation" and those with
103 periodontitis as "severe inflammation". While gingivitis is reversible with proper dental hygiene,
104 periodontitis is an irreversible, chronic disease state without clinical intervention[36]. A full sample
105 list with clinical information can be found in Supplemental Table 1. A 37-color spectral flow
106 cytometry panel was utilized to examine phenotype (no stimulation) and functional capacity
107 (following stimulation) of the T cells isolated from gingival tissues (***Figure 1A****, panel and gating;*
108 *Supplemental Figure 1-2*). As a technical control, a PBMC sample from a single leukapheresis
109 donor was included in every flow cytometry experiment (*Supplemental Figure 3*).

110 We first examined the frequency of T cells (CD3+ cells) within the CD45+ cell compartment
111 and found no changes between mild, moderate, and severely inflamed gingival tissue (***Figure***
112 ***1B***). Of note, a small population of naïve T cells (CCR7+ CD45RA+) was present in each tissue
113 sample. These naïve T cells presumably stem from the blood that is inherently present in tissues.
114 We excluded these naïve T cells from our manual gating analysis approach. We next assessed if
115 T cell subset composition is altered with inflammation. We gated on T cells by first defining innate-
116 like T cell subsets within the CD3+ population, followed by subsetting the remaining CD4 and
117 CD8 T cells into conventional CD4 T cells (CD4 Tconv), regulatory CD4 T cells (Treg), CD103+

118 (tissue-resident phenotype) CD8 T cells and CD103- (circulating) CD8 T cells (*Supplemental*
119 *Figure 1B*). We observed stable frequencies of most T cell subsets, including CD4 Tconv, CD4
120 Treg, and CD103+ CD8 T cells (***Figure 1C***). We noticed a slight reduction in CD103+ CD8 T cells
121 within the total T cell population ($p = 0.1026$), but a significant increase in circulating CD103- CD8
122 T cells in severely inflamed tissue compared to mild inflammation (***Figure 1D***).

123 We next examined if the expression of activation, co-stimulation, and exhaustion markers
124 change with inflammation severity to look for evidence of inflammation-driven (bystander)
125 activation. To visualize similarities and differences in expression of multiple proteins across
126 different tissues, we chose a heatmap-based approach to displaying expression frequency. For
127 each protein, the mean expression frequency is shown on all heatmaps, and the median and data
128 range for each protein are shown in *Supplemental Table 2.* Within conventional CD4 and CD8
129 subsets, we observed only few changes between mild, moderate, and severely inflamed gingiva
130 (***Figure 1E***). Pro-inflammatory cytokines can activate memory T cells and increase the expression
131 of CD69, PD-1, and induce expression of GzmB[20], but we did not observe an inflammation-
132 associated increase of these proteins (***Figure 1E***). On the contrary, we noted reduced expression
133 of CD69 in both the CD8 CD103+ and CD103- populations in severely inflamed compared to
134 mildly inflamed tissues. In the CD4 Tconv population, there were no differences in these
135 phenotypic markers. In general, we observed relative phenotypic stability across inflammation
136 status within each T cell subset (*Supplemental Figure 4*).

137 Next, we examined innate-like T cell subsets including MAIT and $\gamma\delta$ T cells, which can
138 also be activated by pro-inflammatory stimuli[37,38]. While there were no statistically significant
139 differences in MAIT cell frequencies and phenotypic markers across inflammation status, we
140 found a significant reduction in $\gamma\delta$ T cells in severely inflamed compared to moderately inflamed
141 tissue (***Figure 1F***). Within the moderately inflamed condition, we also observed a pronounced
142 reduction of PD-1 expression in the $\gamma\delta$ T cell population (***Figure 1G***). The concomitant increase

143 in the abundance of γδ T cells (as a % of CD3+ T cells) and decreased PD-1 expression could
144 potentially be due to recruitment of γδ T cells from the blood to moderately inflamed tissue. PD-1
145 expression frequency was also significantly higher within CD8 CD103- circulating cells during
146 severe inflammation (***Figure 1E***). While we observed some phenotypic differences in our dataset
147 as tissue became increasingly inflamed, we noted that the T cell profile within all oral mucosal
148 tissues remained rather stable even in severely inflamed tissues. Although we did not observe
149 phenotypic changes indicative of inflammation-driven (bystander) activation of one or more T cell
150 subset in inflamed tissues, we considered that a smaller proportion of T cells may respond in a
151 TCR-dependent manner.
152

153 **Biomarkers of TCR-mediated activation do not significantly change across inflammation**
154 **states in the oral mucosa**

155 We next assessed biomarker pairs indicative of TCR-mediated activation[39-41]. We
156 examined co-expression of CD39+ PD-1+ (for CD8+ cells[41]) as well as ICOS+ PD-1+ (for CD4+
157 cells[39]) across mild, moderate, and severely inflamed oral mucosal tissues. Across gingiva of
158 varying inflammation states, there were no differences in frequency of expression of each of these
159 populations. CD39, PD-1 and ICOS are also expressed on highly activated Tregs, and we
160 consistently observed the highest frequency of expression in CD4 Tregs (***Figure 2A-B***). This
161 suggests that as inflammation within the oral mucosa progresses from mild to severe, there is no
162 evidence for an increase in antigen-mediated responses by T cells. In line with this observation,
163 no changes in Ki67 expression, an indicator of recent cell proliferation, were observed across
164 inflammation status (***Figure 2C-D***). Lastly, we examined TIM3 and PD-1 expression, a biomarker
165 pair indicative of exhaustion, within each T cell subset. We observed unaltered co-expression of
166 these markers regardless of inflammation state, indicating that the lack of observed changes is
167 not due to T cell exhaustion (***Figures 2C-D***). Together, these data indicate that biomarkers of T

168 cell activation and proliferation remained stable across a range of inflammatory disease states
169 within the gingiva. Overall, we did not detect evidence of inflammation- or TCR-driven activation
170 of the T cell compartment in the inflamed gingiva. We considered that this could be the result of
171 a state of T cell dysfunction and thus interrogated T cell functional properties.
172

173 **Functional capacity for T cell-mediated tissue healing and cytokine production is**
174 **maintained in inflamed oral mucosa**

175 To examine how the functional capacity of T cell subsets varies across inflammation, we
176 stimulated T cells isolated from gingival tissue for 6 hours with PMA/ionomycin (***Figure 1A***). We
177 define the functional capacity simply as the ability of a T cell to express protein following this brief,
178 yet broad, activation stimulus. Within CD4 and CD8 subsets, we observed no statistically
179 significant differences in AREG, IFNγ, TNFα, IL-17A, IL-17F, IL-2, or IL-22 (***Figure 3A,***
180 *Supplemental Figure 5*). Overall, there were no changes in the functional capacity of T cell subsets
181 across mildly, moderately, and severely inflamed gingiva (***Figure 3B***). This was also consistent
182 within innate like subsets (***Figure 3C***). The mean, median, and data range are reported in
183 Supplemental Table 2. Within several T cell subsets, we found co-expression of GzmB and AREG
184 upon stimulation (***Figure 3D***), which may indicate dual functional roles (cytotoxicity and tissue
185 repair) can occur simultaneously within the same T cell. The highest frequency of GzmB and
186 AREG co-expression was observed in CD8 CD103+ cells (***Figure 3D***), though these were also
187 detected to a lesser extent in CD4 Tconv, CD4 Tregs, and innate-like subsets (~1% within CD4
188 Tconv, Treg and MAIT cells, ~4% in γδ T cells). The frequencies of GzmB+ AREG+ populations
189 within each T cell subset did not change across inflammation states (***Figure 3D***). Overall, these
190 data suggest T cells retained functional properties even in severely inflamed gingiva, and that
191 inflammation did not disrupt tissue-specific adaptation of the T cell compartment in the gingiva.
192

T cells in both the lung and decidual-placental interference (DPI) display few phenotypic changes by inflammation status, but high variation by tissue origin

We next wanted to assess whether the phenotypic and functional stability of T cells across inflammation states is a gingiva-specific phenomenon or could also be extended to other mucosal tissues in healthy and inflamed states. We decided to examine the lung and the decidual-placental interface (DPI) as a set of mucosal tissues that are inherently very distinct from the oral mucosa in function and commensal exposure[42-44]. We assessed lung samples from deceased adult organ donors (healthy) along with resected lung tissue from patients with interstitial lung disease (ILD) patients. Briefly, ILD is a group of pulmonary disorders causing inflammation and lung tissue scarring[45]. Tissue sampling was performed on both upper and lower lung lobes, which yielded nearly congruent profiles (*Supplemental Figure 6*); the upper lobe data are shown for the remainder of the figures. Decidual-placental interface (DPI) samples were taken from a cohort of term (37-41 weeks gestation), uncomplicated pregnancies (healthy) and a cohort of term pregnancies diagnosed with intra-amniotic inflammation (IAI). IAI, often referred to as chorioamnionitis, is typically an acute inflammatory response to a bacterial infection[46].

First, we examined the composition of the T cell compartment in lung and DPI (***Figure 4A***). T cells isolated from DPI tissues displayed a higher frequency of naïve cells among all CD3+ CD45+, which are likely derived from the highly vascularized placental tissue. These naïve T cells were again excluded from manual gating analysis to facilitate a comparison with the memory phenotype T cells in other tissues. We noted a decrease in MAIT cell ($p = 0.020$) and $\gamma\delta$ T cell ($p = 0.133$) abundance in inflamed over healthy lung (***Figure 4A***). We next quantified the number of markers that are significantly different based on tissue origin vs. inflammation state across each T cell subset. For this, the source of variation from 2-way ANOVA statistical testing (row factor and column factor p values) were counted as significant differences if $p < 0.05$ and totaled for all subsets. We observed that tissue origin had a greater impact on subset composition and phenotypic differences than inflammation status. (***Figure 4B****, Supplementary Table 2, markers*

219 *displayed on heatmaps in Supplemental Figure 7*). We found an inflammation-associated,
220 statistically significant increase in CD69+ T cells within several subsets, specifically, CD4 Tregs,
221 CD8 CD103+, and CD8 CD103- T cells in the placenta, but not the lung (***Figure 4C**, Supplemental*
222 *Figure 7, statistical analysis across tissues excluded from heatmaps*). False discovery rate
223 corrections for multiple comparisons of lung and placenta phenotype were also performed
224 (*Supplemental Table 3*). The most profound inflammation-associated phenotypic change
225 occurred within T cells in the lung. We observed a dramatic reduction in CD25 expression on all
226 T cell subsets in inflamed lungs (***Figure 4C***). Similarly to the oral mucosa, we did not observe an
227 increase in GzmB in healthy vs. inflamed tissues (lung and DPI) (***Figure 4C***). Furthermore, there
228 was no evidence of inflammation-associated activation of T cells, TCR-mediated activation,
229 proliferation, or exhaustion (*Supplemental Figure 8*), but rather, tissue origin predominantly
230 shaped the general phenotypic profile of T cell subsets.

231 To further visualize this relationship of phenotype and tissue location vs. inflammation
232 state across all three tissue sets, we grouped all datapoints from each tissue (irrespective of
233 inflammation state), color-coded each datapoint according to inflammation state, and compared
234 the expression of T cell surface markers across gingiva, lung, and placenta within conventional T
235 cell subsets (***Figures 4D-F***). As highlighted in previous figures, we did not observe inflammation-
236 associated changes in GzmB expression in CD8 T cell subsets, however there was a significant
237 difference in GzmB expression in CD8 CD103- T cells in the gingiva compared to lung and DPI
238 (***Figure 4D***). Among these tissue sets, the gingiva is presumably the tissue that is most
239 consistently and substantially exposed to microbes and antigen yet still displayed the lowest
240 baseline GzmB expression in CD8 CD103- T cells. Similarly, the frequency of TIM3+ Tregs was
241 lowest in the gingiva (***Figure 4E***). TIM3 expression by Tregs is typically observed in highly
242 activated Tregs in the tumor microenvironment[47]. In our dataset, we observed a nearly 3x increase
243 in frequency of TIM3 expression in Tregs from the DPI compared to gingiva (***Figure 4E***).
244 Together, these data suggest that the DPI, although typically considered to be a sterile tissue

245 environment[42], shows signs of being highly activated and highly suppressive. In line with this
246 notion, we also observed the highest frequency of CTLA4+ expressing CD8 CD103+ T cells in
247 the DPI (***Figure 4F***). Together, these data highlight that tissue-specific adaptions in the T cell
248 compartment exist across these 3 mucosal tissues and were maintained during states of
249 inflammation. We next wanted to test if the maintenance of tissue-specific adaptation also
250 extended to the functional capacity of these T cell subsets.
251
252 **Functional capacity of T cells is primarily shaped by tissue location**
253 As a first step, we examined the functional capacity of T cell subsets across lung and DPI
254 during health and disease. We found that the expression pattern of cytokines was relatively stable
255 across inflammatory states. Two statistically significant changes between healthy and inflamed
256 lung were noted in CD4 Tconv; a decrease in IL-17A and IL-17F expressing cells in inflamed
257 lungs (***Figure 5A****, Supplemental Figure 9, statistical analysis across tissues excluded from*
258 *heatmaps*). Full statistical testing (FDR corrections for multiple comparisons is detailed in
259 Supplementary Table 3. CD4 Tconv from the DPI expressed more IL-2 compared to their lung
260 counterparts, regardless of inflammation status (***Figure 5A***). Overall, we observed for several T
261 cell populations (CD4 Tconv, CD8 CD103+, and CD8 CD103-) from the DPI that they express
262 more IFNγ and TNFα compared to lung (***Figure 5A***).
263 We next compared the functional capacity across all three tissue sites and inflammation
264 status, (***Figure 5B****, gingiva – top, circles; lung – middle, triangles; placenta – bottom, diamonds*).
265 These data highlight that the greatest capacity for T cell IFNγ production (***Figure 5B***, left panel)
266 and IL-2 (***Figure 5B***, middle panel) was observed in the DPI. TNFα was also produced in the
267 highest quantities by T cells from the DPI and lowest in the lung (***Figure 5C***). In contrast, IL-17A
268 expression was essentially absent in DPI T cell subsets and most prominent in the oral mucosa
269 (***Figure 5B***, right panel). Differences in the functional capacity of CD4 Tregs particularly stood out

270 (***Figure 5B).*** The oral mucosa contained a large fraction of Tregs that expressed IL-17A following
271 stimulation (***Figure 5B***, right panel), while Tregs from the placenta expressed IFNγ and IL-2
272 (***Figure 5B***, left and center panels). Of note, we observed co-expression of IFNγ and IL-2 for both
273 CD4 Tconv and Tregs from the DPI (***Figure 5D***) thus potentially suggesting that FoxP3+ CD127-
274 T cells may be activated CD4 Tconv (explored further in the discussion). Finally, it is noteworthy
275 that the bias towards certain functional properties in each tissue set was mirrored across several
276 T cell subsets. For example, gingival Tregs were the most potent IL-17 producers, and this was
277 true for CD4 T cell subsets, but also MAIT cells and γδ T cells (***Figure 5B***) regardless of
278 inflammation status. Overall, these data support the notion that the functional capacity of T cell
279 subsets is linked to tissue location, and that this can be maintained during inflammatory disease.
280

281 **Functional potential of T cells groups by tissue and not inflammatory status in**
282 **dimensionality reduction analysis**

283 Our analysis approach so far was focused on specifically examining select biomarkers of
284 activation and functional properties**.** We next wanted to compare tissues in a more unsupervised
285 analysis approach that takes the expression pattern of all proteins assessed in our 37-color panel
286 into account. Of note, we included all phenotypic and functional markers in the antibody staining
287 panel in this PCA analysis (TIM3, CD39, ICOS, CD25, CD28, CD27, PD1, Ki67, IL1R1, CD137,
288 CD40L, CTLA4, IL-2, IL-22, AREG, IL-17A, IFNγ, GzmB, TNFα, IL-17F). We first used principal
289 component analysis (PCA) to again compare the effect of tissue origin vs. inflammation status on
290 T cell function (***Figures 6A-D****, Supplemental Figure 10)*. Tissue-based differences were
291 particularly apparent in CD4 Tconv and CD8 CD103+ T cells (***Figures 6A- B***) and were somewhat
292 less pronounced in MAIT and γδ T cells (***Figures 6C-D***). In contrast, for all subsets, there was
293 near congruent clustering based on inflammation status.

294 When determining which parameters are contributing most to determining the principal
295 components (loading scores), upon stimulation, changes in IFNγ among all T cells contributed the
296 greatest. The co-stimulation markers CD27 and CD28 were also significant contributors to the
297 PCA. Importantly, similar findings were observed when PCA was performed with samples directly
298 *ex vivo* (*Supplemental Figure 11)*. Taken together, an unsupervised analysis approach further
299 underlines the notion that tissue inflammation is not sufficient to disrupt tissue-specific
300 adaptations.
301
302 **Unsupervised analysis approaches highlight that tissue-adaptation is the primary driver**
303 **of phenotypic and functional T cell changes**
304 We next wanted to use an unsupervised approach to assess the relative abundance of T
305 cells with functional similarity across tissue and inflammation state. An unsupervised approach
306 allows for discovery of unique populations missed by manual gating of each marker using single-
307 or double-positive gates. For this approach, we included naïve T cells in the analysis as a
308 reference population. Briefly, we defined cell types by manual gating, performed
309 scaling/normalization, and defined global clusters across all batches. (described further in
310 methods). We assessed each T cell subset using this approach with tissues *directly ex vivo* and
311 following stimulation. We used our technical PBMC control sample within each experiment to
312 ensure that variation over time (antibody staining, flow cytometry set-up, etc.) was not a
313 confounding factor (*Supplemental Figure 3*).
314 Given the profound functional differences of Tregs between tissues, we initially focused
315 our analysis on Tregs upon stimulation. We observed ten distinct population clusters; the
316 expression of each marker is represented in the bubble plot (***Figure 7A***). Clusters 1 and 4 were
317 comprised of naïve cells based on the expression of CD45RA+ CCR7+, whereas the remaining
318 clusters consisted of memory subsets.

319 When examining cluster frequencies across tissues (gingiva, pink; lung, green; placenta,
320 purple) and noted distinct clustering based on tissue origin, described further below (***Figure 7B***,
321 *top panels*). We also examined cluster frequencies across inflammation status (healthy, blue;
322 inflamed, red), and observed relative stability (***Figure 7B,*** *bottom left panels*).

323 Cluster 5, characterized by high expression of TNFα, was most abundant within the oral
324 mucosa (***Figure 7C-D***). Cluster 6 contains cells that express the proliferation marker Ki67 and
325 was found in high frequencies among placental tissues. Cluster 7, which comprised a large
326 proportion of all Tregs, is made up of cells that express CD39 and few other cytokines and was
327 prevalent in most samples, but most abundant in the placenta. Cytokines IFNγ and IL-17A are
328 represented within clusters 8 and 10, respectively. Tregs from the DPI during both health and
329 inflammation that group with cluster 8 are increased compared to gingiva and lung Tregs (***Figure***
330 ***7D***). Cluster 10, characterized by the expression of IL-17A and IL1R1, was highest in the gingiva
331 (***Figure 7C-D***). Though markers like CTLA-4 increase upon stimulation with PMA/ionomycin, our
332 normalization methods allow for comparison of positive cells and comparison across groups.
333 Overall, these data are in line with our supervised analysis (***Figure 5B****, Supplemental Figure 9*).

334 We also examined how CD4 Tconv cells cluster across tissue and inflammation
335 (*Supplemental Figure 12*). Here, cluster 8 contains IL-17A+ Tconv cells (*Supplemental Figure*
336 *12A*). This cluster was most abundant within Tconv from gingival samples (*Supplemental Figure*
337 *12D, bottom right panel*). To summarize all clustering data for other T cell subsets *ex vivo* and
338 upon stimulation, we used clustering frequencies to generate PCA plots (*Supplemental Figure*
339 *13-14*). When cluster frequencies were used to determine principal components, distinct tissues
340 (gingiva, lung, and DPI) form unique groups, whereas healthy and inflamed tissues overlap.
341 Overall, our unsupervised analysis approach highlights that clusters show tissue-specific
342 distribution with minimal perturbation based on the inflammation status.

343 In summary, across all analysis methods, we found that tissue-specific adaptations of T
344 cell subsets were maintained during tissue inflammation.

Discussion

Our main goal was to assess the extent to which tissue-specific adaptations of T cell subsets are altered during tissue inflammation. We were surprised that markers indicative of inflammation-driven T cell activation did not significantly change in most T cell populations, including MAIT and $\gamma\delta$ T cells, as inflammation severity of the gingiva increased. We considered that this could be due to the baseline level of inflammation that is present even in healthy gingival tissues[35], which could yield unique regulatory mechanisms in the tissue. Since the oral mucosa is colonized by a dynamic microbiome and continuously exposed to dietary and microbial antigens[35], we also examined the expression of biomarker pairs that indicate TCR-mediated activation. ICOS and PD-1, and CD39 and PD-1 have been shown to be indicative of recent TCR activation for human CD4 and CD8 T cells, respectively[39-41]. Neither of these biomarker pairs indicated an association of a TCR-mediated T cell response in CD4 Tconv or a CD8 T cell subset gingiva with increased severity in inflammation. Similarly, Ki67 expression, an indicator of cell proliferation, and expression of PD-1 and TIM3, indictors of T cell exhaustion, did not change with increased inflammation in the gingiva. Overall, our observations highlight that the overall composition, phenotypic, and functional properties of T cell subsets in the gingiva were retained at various states of inflammation.

Because of the unique physiological demands of the gingiva, such as mastication, we asked if the T cell compartment would be similarly resistant to inflammation-mediated changes in other mucosal tissues, specifically the lung and the DPI. CD4 Tconv and CD8 T cell subsets in the healthy lung did not express these biomarker pairs of TCR activation. However, in the DPI we found that a substantial fraction of CD4 and CD8 T cell subsets co-expressed ICOS and PD-1, and CD39 and PD-1, respectively (*Supplemental Figure 8*). These data suggest that T cells in the DPI encounter their antigen more frequently than T cell in the gingiva and lung. This could potentially be related to the presence of fetal-derived, semi-allogenic tissue (the placenta is

370 made of fetal-derived trophoblasts) or could indicate that recently activated T cells migrate to
371 the DPI to provide protection. An in-depth analysis of the TCR repertoire in the DPI compared to
372 other tissues may provide a more definitive answer in future studies. Finally, ICOS, CD39 and
373 PD-1 are all expressed by highly activated Tregs, and expression of these markers was found
374 on a large fraction of Tregs across all tissues and inflammation states.

375 Given the presence of highly activated Tregs in all tissues, we explored potential
376 functional differences. We found that in gingival tissues, regardless of inflammation status,
377 about 10% of Tregs expressed IL-17A. IL-17+ Treg have been previously described and are
378 thought to maintain their ability to suppress other T cells, while secreting IL-17 in response to
379 TCR-mediated activation, or IL-6 and IL-1β stimulation[48,49]. In contrast, we did not observe IL-
380 17+ Tregs in lung or DPI. However, we found that a fraction of Tregs in both healthy and
381 inflamed DPI could express IFNγ, while none of the Tregs in other tissues expressed IFNγ
382 following stimulation. These cells could be Th1-like Tregs that have so far been mainly
383 described in peripheral blood in context of human autoimmune diseases and are thought to be
384 hypo-suppressive[50]. Thus, our observation could indicate that these Tregs also exist in a healthy
385 human tissue (albeit from a unique environment that contains a semi-allogeneic tissue), but it
386 important to consider that these could also be recently activated Th1 cells that temporarily
387 express FoxP3[51]. Follow up studies will be required to transcriptionally define this DPI-enriched
388 CD4 T cell population. Overall, tissue-associated phenotypes and functional properties were
389 evident, while inflammation-associated changes were limited in our cross-tissue comparison.

390 The most prominent phenotypic changes that we observed between a healthy and
391 inflamed tissue was the striking decrease in CD25 expression on T cell subsets in the inflamed
392 lung (Figure 4C, *Supplemental Figure 7*). We used a technical batch control to rule out any
393 technical artifacts. Previous reports indicated an increase in serum soluble CD25 levels in
394 individuals with ILD (both granulomatous-lymphocytic and rheumatoid-arthritis associated

395 ILD)[52,53]. ILD has also been clinically associated with increased matrix metalloproteinase (MMP)
396 expression in serum[54,55], which cleaves CD25 from the surface of T cells. If there is a local
397 increase in MMP activity in ILD lungs, then this could provide an explanation of the decreased
398 CD25 during ILD in all T cell subsets.

399 We specifically looked for functional changes that have previously been associated with
400 inflammation status. Studies using gingival tissue indicated a potential association between
401 inflammation and the abundance of Th17 cells[56,57]. We found that the overall composition of the
402 T cell compartment, including the frequency of CD4 T cells that make IL-17A or IL-17F following
403 stimulation, is stable even during inflammation. It is important to keep in mind that a hallmark
404 feature of inflammation is the recruitment of immune cell populations to a site of inflammation,
405 and that inflammation of the gingiva is associated with an increase in T cell infiltration[58]. Thus,
406 while the overall number of T cells with a specific function increases in inflamed tissues, this is
407 not necessarily associated with a skewing in functional properties within the T cell compartment.
408 Overall, the composition of the T cell compartment was consistent between mildly to severely
409 inflamed gingiva, with few subsets showing an increase or decrease with inflammation.
410 Specifically, we observed a reduction in resident CD8 CD103+ T cells within more severely
411 inflamed gingival tissue with a concomitant proportional increase in circulating CD8 CD103- T
412 cells. This stable maintenance of function would presumably change, at least temporarily, in
413 disease-specific conditions with an associated antigen-specific T cell response, such as the
414 Th17-driven response against *Candida albicans* and *Staphylococcus aureus*[59].

415 We conclude from these data that a state of tissue inflammation does not per se override
416 tissue-specific features of the T cell compartment. Importantly, our observations for the T cell
417 compartment do not necessarily extend to inflammation-associated alterations of other cell
418 types, particularly innate immune cells, in these tissues. In the gingiva, it is well documented
419 that neutrophil infiltration is associated with acute inflammation[56,60,61]. In the lungs, similar innate

420 subsets of macrophages and neutrophils have been reported to drive inflammatory responses in
421 mice and humans[62,63], and acute chorioamnionitis has also been defined by neutrophil
422 infiltration[64]. Furthermore, it is important to keep in mind that specific diseases can profoundly
423 impact T cell phenotype and function during inflammation. Thus, while our data indicate that
424 tissue inflammation is not inherently sufficient to override tissue-specific T cell adaptation,
425 different disease settings may display profound T cell changes such as previously observed in
426 the context of Hepatitis A infection, which leads to increased IL-15 availability and bystander
427 activation of CD8 T cells[27].

428 Finally, we want to highlight that we used a brief PMA/Ionomycin stimulation condition to
429 examine the functional capacity of T cells. We reasoned that the broadly activating nature of this
430 stimulus will reveal which proteins T cell subsets are able to express, while keeping in mind that
431 it does not reveal which proteins are secreted in situ. This approach indicated that T cell subsets
432 retained their ability to express AREG even in chronically inflamed tissue such as the ILD lung
433 and severely inflamed gingiva. Whether AREG is actually secreted *in situ* by T cells to promote
434 epithelial cell recovery in the inflamed gingiva is unclear. CD8 T cells appear to require a TCR
435 signal to secret AREG[34] and given the lack of evidence for CD8 T cell activation (including TCR-
436 mediated T cell activation) in these tissues, *in situ* AREG secretion by CD8 T cells seems
437 unlikely. However, given that the functional capacity is maintained in inflamed tissues, novel
438 therapies could target AREG to elicit expression or other specific functional responses.

439 In summary, we report that tissue-specific T cell adaptations can be maintained during
440 states of tissue inflammation. By gaining a more complete understanding of how inflammation
441 affects the tissue-specific T cell landscape, therapeutic approaches can be designed to develop
442 treatments with tissue-specific requirements in mind.

443 # Material and Methods

444 ## Approvals & Study Population

445 *Tissue Samples and Protocols:* All protocols used in this study were approved by the Institutional
446 Review Board (IRB #0008335, 00008263, 00004036, 00001636). Signed informed consent was
447 obtained from all participants. A list of all samples, along with relevant clinical information can be
448 found in Supplementary Table 1. Each sample is from a unique donor.

449

450 *Oral Mucosa:* Oral mucosa samples were obtained from surgically discarded tissue from routine
451 surgeries, such as osseous surgery, functional or esthetic crown lengthening procedures, tooth
452 extractions, or impacted tooth uncover procedures. Mild inflammation (clinical health, mild to
453 moderate gingivitis), moderate inflammation (severe gingivitis, stage I, and stage II periodontitis),
454 and severe inflammation (stage III and IV periodontitis).

455

456 *Lung:* Healthy lung samples were redirected transplants from deceased organ donors. Donors
457 without history of lung disease, infection, and mechanical ventilation for >7 days were eligible for
458 screening. Inflamed lung samples (interstitial lung disease, ILD) were obtained from patients
459 undergoing lung transplant. Explant lungs and hilar lymph nodes were obtained from patients with
460 ILD undergoing lung transplant at the University of Washington.

461

462 *Decidual-Placenta Interface:* Both healthy and acutely inflamed (chorioamnionitis) third trimester
463 placentas were obtained following vaginal delivery or C-section, following labor or no labor
464 (detailed in Supplementary Table 1).

465

466 *Technical Control Sample:* A consistent leukopak peripheral blood mononuclear cell (PBMC)
467 sample was used throughout each flow cytometry batch and assessed alongside experimental

468 samples to ensure longitudinal control. Leukopak (4510-01 Ful Leuko Pack) obtained through
469 Bloodworks Bio (Seattle, WA).
470

471 **Isolation of Lymphocytes from Tissues**

472 *Oral Mucosa:* Following procedures, mucosal tissue was priority shipped overnight with cold
473 packs to Fred Hutch Cancer Center (FHCC). Upon arrival, tissue was washed with complete
474 media (RPMI1640 (11875-093, Gibco) with penicillin, streptomycin (15140-122, Gibco), and 10%
475 fetal bovine serum (FBS, PS-FB2, Peak Serum)). An optimized protocol was adapted from
476 reference[65], originally developed for processing solid tumors. Tissue was placed in a petri dish
477 and minced with a scalpel, then enzymatically digested (Collagenase II (C6885, Sigma-Aldrich),
478 DNAse (20 units/ml, #D502, Sigm) in complete media with reduced 7.5% FBS (RP7.5) in a 25 mL
479 volume at 37°C for 40 minutes while shaking. Following digest, the sample was passed through
480 a needle (16x1 ½ Blunt, 302833, BD) 10 times prior to passing through a 100-micron cell strainer.
481 Remaining tissue pieces were mashed using a syringe plunger, washed with complete media,
482 and frozen in 1 mL Recovery Cell Culture Freezing Medium (12648010, Gibco) and stored in
483 liquid nitrogen until future experiments. Cell viability and abundance were quantified prior to
484 freezing by staining a small sample aliquot (Guava antibodies 7-AAD, CD19, and CD45) for 15
485 minutes, resuspension in 1% PFA, and collection on the Guava easyCyte. Oral mucosa samples
486 in this study contained between 731-52,195 T cells, as analyzed by flow cytometry.
487

488 *Lung:* Lung tissue was processed in a similar fashion to the gingiva using the RP7.5 digestion for
489 50 minutes at 37°C while shaking at 225 RPM. Subsequently cells were washed with RP10,
490 strained through a 70μm filter and enumerated. Lung tissue samples contained between 1,537-
491 62,719 T cells.
492

493 *Decidual-Placenta Interface:* Tissue was processed as previously described[66]. Briefly, intact
494 placentas were biopsied up to a 0.5 cm depth on the maternal facing surface of the placenta
495 including both decidua basalis and placenta villi. Tissue was digested in digestion media (above)
496 and incubated at 37°C for 60 minutes with agitation. Concentration for digest was RP7.5 + 700
497 U/mL Collagenase Type II (Sigma-Aldrich) and 200 U/mL DNase. Cells were filtered and washed
498 with media. Red blood cells were removed using ACK lysis buffer, followed by resuspension with
499 media. Maternal blood was collected in tubes containing the anti-coagulant acid citric dextrose.
500 DPI tissue samples contained between 10,303-102,650 T cells.
501
502 *Technical Control Sample:* Leukopak was processed according to StemCell Technologies
503 protocol (https://www.stemcell.com/leukopak-processing-protocol.html). Two blood cell lysis
504 steps at room temperature and two platelet washes were performed prior to counting and freezing
505 20 million cells per aliquot.
506

507 **Stimulation Assay**

508 As briefly outlined in Figure 1A, upon experimentation, cryo-preserved single-cell suspension
509 isolated from tissues or blood (outlined above) were thawed in a 37°C water bath. 12,000 to 2
510 million cells per condition were plated in a U- or V-bottom 96 well plate in 200 uL complete media.
511 For assessing phenotype directly *ex vivo*, cells were left untreated for 2 hours at 37°C. GolgiStop
512 (Monensin, 554724, BD) and GolgiPlug (Protein Transport Inhibitor (Containing Brefeldin A),
513 555029, BD) were then added per manufacturer recommendations to compare directly to
514 stimulated samples and was returned to the 37°C incubator for 4 more hours (total of 6 hours).
515 During functional stimulation assays, samples were similarly thawed and plated. 200 uL complete
516 media supplemented with PMA (100 ng/mL, P8139, Sigma) and ionomycin (1000 ng/mL, I9657,
517 Sigma) for 6 hours, including the addition of Golgi stop/plug 2 hours after beginning the
518 stimulation. Upon completion, samples were stained for analysis by flow cytometry.

519

520 **Spectral Flow Cytometry**

521 *Staining:* For all experiments, upon completion of the assay, samples were stained previously
522 described[67]. Prior to experimentation, the spectral flow panel was tittered, optimized, and tested
523 to ensure proper design and maximal information could be obtained from each sample, as
524 detailed in reference[68]. All staining steps were performed in the dark at room temperature in a 96-
525 bottom plate. Cells were incubated with FcX block (422302, Biolegend) and Zombie NIR dye
526 (422302, Biolegend) in PBS (14190250, Gibco) for 15 minutes. Antibody master mixes were spun
527 down at 10,000xg for 4 minutes prior to staining to remove aggregates. Following live/dead
528 staining, cells were washed, following by surface staining in 50uL (antibody mix in PBS + 2% FBS
529 and 10% brilliant stain buffer (563794, BD)) for 20 minutes. Cells were then washed twice prior to
530 fix/perm (100 uL, 554722, BD) according to manufacturer guidelines for 30 minutes. After fixation,
531 cells were stained intracellularly for select markers noted in the panel (Supplementary Figure 1)
532 for 30 minutes, assembled in perm/wash buffe and 10% BSB. Finally, cells were washed twice
533 with perm/wash and resuspended in PBS + 2% FBS and stored at 4°C until acquisition the
534 following day on the BD Discover S8.

535

536 *Controls*: Single-stain controls were optimized for individual markers by staining either
537 unstimulated PBMCs, PBMCs following a 6-hour PMA/ionomycin stimulation, or unstimulated
538 control tissue samples (generally tonsil tumor infiltrate or regional lymph nodes). For two markers
539 expressed in low abundance in PBMC and tissue (IL-13 and IL-22), capture beads were used for
540 single-stain control. Control samples were taken through an identical staining protocol to
541 experimental samples, described above. A reference sample was also used within each
542 experiment as a longitudinal control (*Supplemental Figure 3*).

543

544 *Cytometer*: Data from all experiments was collected with the BD Discover S8 and the
545 FACSChorus software platform (BD Biosciences). The S8 is equipped with 5 lasers and 78
546 detectors. Compensation controls were prepared and used for each individual experiment, aside
547 from one run containing ILD 11 and 12. Upon collection, data was exported (FCS 3.1 format) and
548 analyzed using FlowJo version 10.10.0. Files were analyzed in batches by collection day, with
549 minor gating changes across different batches.
550

551 **Unsupervised Clustering**

552 Upon acquisition on the Discover S8 (BD), samples were gated (*Supplemental Figure 1*).
553 Following gating of time, lymphocytes, single cells, and live cells, T cells were gated (CD3+
554 CD45+) and exported as a new .fcs file in FlowJo. Files were also stripped of parameters out of
555 scope for this analysis, focusing on time, size channels, and those containing a fluorochrome
556 (*listed in Supplementary Figure 1*). Upon creation of files containing only T cells, separate streams
557 were created for each relevant T cell subset assessed in this study: $\gamma\delta$ T cells (TCR$\gamma\delta$+), MAIT
558 cells (CD161+ Vα7.2+), all CD4 (CD8-), Tconv (FoxP3-), Tregs (FoxP3+ CD127-), all CD8 (CD8+
559 CD4-), resident CD8 cells (CD103+), and circulating CD8 cells (CD103-). Naïve cells were
560 included in clustering analysis for all tissues.

561 We included additional samples in our clustering analysis as reference tissues for tissue-
562 enriched T cell subsets (*Supplemental Table 1, gray lines*). Lung and associated lymph nodes,
563 along with maternal blood from placental donors were included in multiple batches. We also
564 included tumor infiltrates from head and neck squamous cell carcinoma (HNSCC) and associated
565 lymph nodes. One experimental batch did not include marker CD127 and was excluded from the
566 Tconv and Treg clustering analyses (n = 1 pediatric lung and associated LNs, 2 inflamed lungs
567 and associated LNs, 2 tumor infiltrate samples, and 8 tumor associated LNs).

568 For each clustering stream, we used up to 20,000 T cells per sample. No minimum cell
569 threshold was utilized. Actual T cell counts for individual samples and primary clustering streams
570 were considered for count analysis. The following markers were used to develop clusters: CD161,
571 CD39, CCR7, ICOS, CD25, IL-17F, CD28, CD27, CD45RA, PD-1, Ki67, CD69, TIM3, IFNγ,
572 CTLA4, IL-13, IL-22, GzmB, TNFα, IL1R1, CD137, AREG, CD40L, IL-17A, CD45RO, IL-2.
573 Lineage markers and QC parameters were excluded from clustering analysis: CD3, CD45, CD4,
574 CD8, FoxP3, CD127 or CXCR5, CD103, TCRγδ, Vα7.2, Live/Dead, Autofluorescence. Spectre[69]
575 was used to determine appropriate arcsinh transformation values for each parameter.
576 Repeated clustering at the single cell level – necessary to identify and factor out technical
577 noise, or perceived batch effect – is computationally intractable at the scale of this study.
578 Therefore, within each of the streams, to arrive at globally defined clusters across all batches, we
579 cluster the centers of clusters from batch-specific clusterings[70,71]. Specifically, we 'over'-cluster
580 within each batch by first clustering, then subclustering the cells within each cluster. Next, we
581 compute the centroids of all (sub)clusters in each batch and cluster these (sub)cluster centroids
582 (or "metacells'' or "supercells") to arrive at a global (meta)clustering assignment for each metacell
583 from each batch[72]. At each stage we use the Rphenograph algorithm, with Leiden clustering of
584 shared nearest-neighbor graphs[73,74]. To address moderate drift across batches in some
585 parameters, we first align repeated control median transformed intensity values across batches
586 for select parameters, and next apply the same batch- and parameter-specific shifts to the
587 samples before metaclustering. We use Uniform Manifold Approximate Projection (UMAP) for
588 dimension reduction and data visualization within an iterative process of adjusting for perceived
589 batch effects, optimized by refining the metaclustering at a fixed Leiden resolution, before pushing
590 resolution higher[75].
591
592

593 **Statistical Analyses**

594 Statistical testing was performed using GraphPad Prism Software version 10.5. Testing us noted
595 within figure legends. All bar graphs represent the mean with standard deviation. Heatmaps
596 display the mean for each marker for a given sample group. For oral mucosa samples (*Figures*
597 *1-3*), significance was determined by testing using ordinary one-way ANOVA with Tukey's multiple
598 comparisons test. For lung and placenta data (*Figures 4-5*), 2-way ANOVA was utilized with
599 Tukey's multiple comparisons if comparing two tissues across inflammation states, or one-way
600 ANOVA if comparing with three tissues with grouped inflammation. All data using one-way
601 ANOVA was also assessed using the Benjamini-Hochberg false discovery rate (FDR) correction
602 with a rate of 10% and maintained statistical significance. Supplementary Table 2 used 2-way
603 ANOVA to compare lung and placenta across inflammation; the Benjamini-Hochberg FDR
604 correction with a rate of 10% was utilized.

605 ## Resource Availability

606 Raw flow cytometry files (.fcs) will be available on ImmPort in Study SDY3484.

607 ## Acknowledgements

608 We thank the Flow Cytometry Shared Resources Core at Fred Hutch Cancer Center. We thank
609 Quinn Peters who provided and assisted with the R script used for PCA and Veronica Davé who
610 consulted on proper statical testing and corrections to be used for these analyses. We also
611 thank all members of the Prlic Lab for critical feedback and discussion.

612 ## Author contributions

613 Conceptualization: N.B.P., M.P. Methodology: N.B.P., H. R. M., M.P. Conducting experiments:
614 N.B.P., E. D. V., A. K. T., C. S. D., G. D. Formal analysis: N.B.P., H. R. M., M.P. Writing; original
615 draft: N.B.P., M.P. Writing; review and editing: all authors. Visualization: N.B.P., H. R. M., M.P.
616 Funding acquisition: N.B.P, M.P. Supervision: M.P.

617 ## Funding

618 NIH grants R56DE032009, R01AI123323 and R01AI179712 (to M.P) and funding from the Oral
619 Mucosa Immunology Consortium at the University of Nebraska (to N.B.P, Windsweep Farm
620 Scholar) supported this work.

621 ## Declarations of interest

622 The authors declare no competing interests.

Supplemental Information

Document S1. Figures S1-S14.

Tables S1-3 contain tissue information, data range of heatmaps, and statistical testing.

626 # Figure Legends

627 **Figure 1: The inflammation state in the oral mucosa has a moderate effect on composition**
628 **and phenotype of the T cell compartment.**

629 **A.** Experimental layout, described in detail in methods. Briefly, oral mucosa tissue of varying
630 inflammation states was sent from the clinic to lab, kept at 4°C. Tissue was digested mechanically
631 and enzymatically prior to storage of cryovials with single cell suspension in liquid nitrogen. Upon
632 experiment, samples were thawed and assessed directly ex vivo (*Figures 1-2*) or following a 6h
633 PMA/I stimulation at 37°C (*Figure 3*). **B.** Frequency of CD3+ T cells of CD45+ cells across
634 inflammation state, pre-gated on lymphocytes, single cells, and live (*Supplementary Figure 1*). **C.**
635 Of CD3+ CD45+ cells, frequency of each T cell subset. **D.** Frequency of subset (left to right,
636 CD8+ CD103+ resident, and CD8+ CD103- circulating) of CD3+ CD45+ T cells across
637 inflammation state. For **B-D.** T cell subsetting, n = 9 mild, 13 moderate, 11 severely inflamed oral
638 mucosa tissues. **E.** For each conventional subset, heatmaps depict frequency of activation
639 markers across inflammation status. Phenotyping of T cell subsets must meet minimum 25 cell
640 threshold; sample size is consistent with above unless noted; n = 8 mild, 11 moderate for Tregs.
641 Tconv, CD103+ and CD103- all met minimum threshold. **F.** Frequency of MAIT cells and $\gamma\delta$ T
642 cells of CD3+ CD45+ T cells. **G.** For innate-like T cells, frequency of activation markers across
643 inflammation. Minimum threshold of 25 cells; n = 7 mild, 9 moderate for MAIT cells; n = 8 mild for
644 $\gamma\delta$ T cells. For all plots, ns (not significant), *$p < 0.05$, ***$p < 0.001$, ****$p < 0.0001$ by ordinary
645 one-way ANOVA with Tukey's multiple comparison test.

646

647 **Figure 2: Biomarkers of T cell receptor (TCR)-mediated activation do not significantly**
648 **change across inflammation states in the oral mucosa.**

649 **A.** Expression of CD39+ PD-1+ (right) and ICOS+ PD-1+ (left) among all T cell subsets across
650 inflammation (blue, mild; yellow, moderate; red, severely inflamed). No statistical differences

651 within each subset across inflammation. **B.** Representative flow cytometry plots of CD39
652 (BUV615) by PD-1 (BV605) expression (top) and ICOS (BUV737) by PD-1 (BV605) expression
653 (bottom) within CD4 Tconv cells isolated from severely inflamed oral mucosal tissue. **C.** From left
654 to right, expression of Ki67+ and TIM3+ PD-1+ across T cell subsets across inflammation status.
655 No statistical differences within each subset. **D.** Representative flow cytometry plots of Ki67
656 (BV650) expression (top) and TIM3 (BB515) by PD-1 (BV605) expression (bottom) within CD4
657 Tconv cells isolated from moderately inflamed (top) or severely inflamed (bottom) oral mucosal
658 tissue. No significant differences by ordinary one-way ANOVA with Tukey's multiple comparison
659 test.
660
661 **Figure 3: Functional capacity of T cell subsets is maintained in inflamed oral mucosa.**
662 **A.** Within T cell subset, expression of each molecule across mild, moderate, or severely inflamed
663 oral mucosa following 6h PMA/I stimulation. n = 9 mild, 13 moderate, 11 severely inflamed oral
664 mucosa tissues, unless noted based on minimum threshold for analysis of 25 cells. For Tregs, n
665 = 8 mild; n = 11 moderate. No statistical differences across inflammation status for each marker.
666 **B.** Expression of AREG, IFNγ, and IL-2 within each T cell subset; no statical differences across
667 inflammation. **C.** Expression of each molecule within MAIT and γδ T cells. **D.** Representative
668 gating of AREG+ GzmB+ populations within mildly inflamed oral mucosa (left) and co-expression
669 of AREG+ GzmB+ among CD103+ CD8+ resident T cells (right). For MAIT cells, n = 7 mild, n =
670 8 moderate, n = 10 severe; γδ T cells, n = 7 mild, n = 10 severe. No significant differences by
671 ordinary one-way ANOVA with Tukey's multiple comparison test.
672
673 **Figure 4: T cells subsets from the lung and decidual-placental interference (DPI) display**
674 **few phenotypic changes by inflammation status, but high variation by tissue origin.**

675 **A.** Among all CD3+ CD45+ cells, frequency of indicated subset within each tissue and disease
676 state. **B.** Statistical differences within tissue type and across inflammation by 2-way ANOVA
677 (overall row and column factors). **C.** For conventional subsets (right to left; Tconv, Treg, CD103+
678 CD8+ and CD103- CD8+), frequency of activation markers by tissue and disease status. Unless
679 noted, n = 4 healthy lung, n = 10 inflamed lung, n = 10 healthy placenta, n = 8 inflamed placenta.
680 Some samples did not meet minimum threshold of 25 cells; for Tregs, n = 3 healthy lung; within
681 CD103+, n = 3 healthy lung for all figure panels. Within one experiment, n = 8 inflamed lung
682 samples for Tconv and Tregs for this and remaining panels. Statistical testing between tissues is
683 excluded from heatmaps. **D.** Frequency of GzmB+ cells among CD8 CD103- across tissue and
684 inflammation state (healthy/mild = blue squares, moderate gingiva = yellow circles,
685 severe/inflamed = red diamonds). **E.** Frequency of TIM3+ Tregs. **F.** Frequency of CTLA-4+ cells
686 among resident CD8 CD103+ cells. Pre-gated as indicated in Supplemental Figure 1 prior to
687 subsetting and single-positive gating. *$p < 0.05$, **$p < 0.01$, ***$p < 0.001$, ****$p < 0.0001$ by ordinary
688 one-way ANOVA with Tukey's multiple comparison test.
689
690 **Figure 5: Functional capacity of T cells is primarily shaped by tissue location.**
691 **A.** Upon 6hr stimulation with PMA/ionomycin, expression of cytokines and tissue healing markers
692 across T cell subsets in the lung and placenta. Unless noted, n = 4 healthy lung, n = 10 inflamed
693 lung, n = 10 healthy placenta, n = 8 inflamed placenta. For Tconv and Tregs, n = 8 inflamed lung
694 samples for this and subsequent figure panels. Statistical testing between tissues excluded from
695 heatmaps. **B.** Within each T cell subset, expression of IFNγ (left), IL-2 (middle), and IL-17A (right).
696 For all panels, circles = gingiva, upright triangle = lung, upside down triangle = placenta; for this
697 and subsequent figure panels, healthy/mild = blue, moderate gingiva = yellow, severe/inflamed =
698 red. For MAIT cells, n = 3 healthy lung and n = 9 inflamed lung samples. **C.** TNFα expression
699 across tissues in CD4 Tconv (left) and CD8 CD103- (right), pre-gated based on Supplemental

700 Figure 1 scheme. **D.** Frequencies of IFNγ+ IL-2+ across tissues in CD4 Tconv (left) and Tregs
701 (right). *p < 0.05, **p < 0.01, ***p < 0.001, ****p < 0.0001 by ordinary one-way ANOVA with
702 Tukey's multiple comparison test.
703
704 **Figure 6: Functional potential of T cells groups by tissue and not inflammatory status in**
705 **dimensionality reduction analysis.**
706 Principal components determined by frequency of positive cells within gates from the following
707 parameters: TIM3, CD39, ICOS, CD25, CD28, CD27, PD1, Ki67, IL1R1, CD137, CD40L, CTLA4,
708 IL-2, IL-22, AREG, IL-17A, IFNγ, GzmB, TNFα, IL-17F. PCA plots of flow cytometry data following
709 6-hour PMA/Ionomycin stimulation from gingiva (pink), lung (green), and placenta (purple) during
710 health (blue) and inflammation (red) organized by tissue type (left) and inflammation status (right)
711 of **A.** CD4 Tconv, **B.** CD8 CD103+, **C.** MAIT cells, **D.** γδ T cells. Moderately inflamed oral mucosa
712 is grouped with inflammation category. Ellipses represent 95% confidence interval.
713
714 **Figure 7: Unsupervised analysis approaches highlight that tissue-adaptation is the primary**
715 **driver of phenotypic and functional T cell changes.**
716 The following markers were used to develop clusters: CD161, CD39, CCR7, ICOS, CD25, IL-17F,
717 CD28, CD27, CD45RA, PD-1, Ki67, CD69, TIM3, IFNγ, CTLA4, IL-13, IL-22, GzmB, TNFα, IL1R1,
718 CD137, AREG, CD40L, IL-17A, CD45RO, IL-2. **A.** Bubble plots of expression of each marker
719 within each cluster among Tregs upon stimulation. Resolution = 0.75. **B.** UMAPs of clusters
720 organized by tissue origin and inflammation status. **C.** Stacked bar graphs representing cluster
721 breakdown for individual samples. **D.** Box plots of frequency of each cluster relative to CD4 Treg
722 counts out of total T cells from each sample.
723

References

1. Sathaliyawala, T., Kubota, M., Yudanin, N., Turner, D., Camp, P., Thome, J.J., Bickham, K.L., Lerner, H., Goldstein, M., Sykes, M., et al. (2013). Distribution and compartmentalization of human circulating and tissue-resident memory T cell subsets. Immunity *38*, 187-197. 10.1016/j.immuni.2012.09.020.
2. Kumar, B.V., Ma, W., Miron, M., Granot, T., Guyer, R.S., Carpenter, D.J., Senda, T., Sun, X., Ho, S.H., Lerner, H., et al. (2017). Human Tissue-Resident Memory T Cells Are Defined by Core Transcriptional and Functional Signatures in Lymphoid and Mucosal Sites. Cell Rep *20*, 2921-2934. 10.1016/j.celrep.2017.08.078.
3. Szabo, P.A., Levitin, H.M., Miron, M., Snyder, M.E., Senda, T., Yuan, J., Cheng, Y.L., Bush, E.C., Dogra, P., Thapa, P., et al. (2019). Single-cell transcriptomics of human T cells reveals tissue and activation signatures in health and disease. Nat Commun *10*, 4706. 10.1038/s41467-019-12464-3.
4. Connors, T.J., Matsumoto, R., Verma, S., Szabo, P.A., Guyer, R., Gray, J., Wang, Z., Thapa, P., Dogra, P., Poon, M.M.L., et al. (2023). Site-specific development and progressive maturation of human tissue-resident memory T cells over infancy and childhood. Immunity *56*, 1894-1909 e1895. 10.1016/j.immuni.2023.06.008.
5. Poon, M.M.L., Caron, D.P., Wang, Z., Wells, S.B., Chen, D., Meng, W., Szabo, P.A., Lam, N., Kubota, M., Matsumoto, R., et al. (2023). Tissue adaptation and clonal segregation of human memory T cells in barrier sites. Nat Immunol *24*, 309-319. 10.1038/s41590-022-01395-9.
6. Wong, M.T., Ong, D.E., Lim, F.S., Teng, K.W., McGovern, N., Narayanan, S., Ho, W.Q., Cerny, D., Tan, H.K., Anicete, R., et al. (2016). A High-Dimensional Atlas of Human T Cell Diversity Reveals Tissue-Specific Trafficking and Cytokine Signatures. Immunity *45*, 442-456. 10.1016/j.immuni.2016.07.007.
7. Niessl, J., Muller, T.R., Constantz, C., Cai, C., Nilsen, V., Rivera Ballesteros, O., Adamo, S., Kammann, T., Mouchtaridi, E., Gao, Y., et al. (2025). Tissue origin and virus specificity shape human CD8(+) T cell cytotoxicity. Sci Immunol *10*, eadq4881. 10.1126/sciimmunol.adq4881.
8. Reina-Campos, M., Monell, A., Ferry, A., Luna, V., Cheung, K.P., Galletti, G., Scharping, N.E., Takehara, K.K., Quon, S., Challita, P.P., et al. (2025). Tissue-resident memory CD8 T cell diversity is spatiotemporally imprinted. Nature *639*, 483-492. 10.1038/s41586-024-08466-x.
9. Traxinger, B.R., Richert-Spuhler, L.E., and Lund, J.M. (2022). Mucosal tissue regulatory T cells are integral in balancing immunity and tolerance at portals of antigen entry. Mucosal Immunol *15*, 398-407. 10.1038/s41385-021-00471-x.
10. Munoz-Rojas, A.R., and Mathis, D. (2021). Tissue regulatory T cells: regulatory chameleons. Nat Rev Immunol *21*, 597-611. 10.1038/s41577-021-00519-w.
11. Miragaia, R.J., Gomes, T., Chomka, A., Jardine, L., Riedel, A., Hegazy, A.N., Whibley, N., Tucci, A., Chen, X., Lindeman, I., et al. (2019). Single-Cell Transcriptomics of Regulatory T Cells Reveals Trajectories of Tissue Adaptation. Immunity *50*, 493-504 e497. 10.1016/j.immuni.2019.01.001.
12. Simon, M., Stuve, P., Schmidleithner, L., Bittner, S., Beumer, N., Strieder, N., Schmidl, C., Pant, A., Gebhard, C., Eigenberger, A., et al. (2024). Single-cell chromatin accessibility and transposable element landscapes reveal shared features of tissue-residing immune cells. Immunity *57*, 1975-1993 e1910. 10.1016/j.immuni.2024.06.015.
13. Gray, J.I., Caron, D.P., Wells, S.B., Guyer, R., Szabo, P., Rainbow, D., Ergen, C., Rybkina, K., Bradley, M.C., Matsumoto, R., et al. (2024). Human gammadelta T cells in diverse

tissues exhibit site-specific maturation dynamics across the life span. Sci Immunol *9*, eadn3954. 10.1126/sciimmunol.adn3954.

14. Kammann, T., Cai, C., Sekine, T., Mouchtaridi, E., Boulouis, C., Nilsen, V., Ballesteros, O.R., Muller, T.R., Gao, Y., Raineri, E.J.M., et al. (2024). MAIT cell heterogeneity across paired human tissues reveals specialization of distinct regulatory and enhanced effector profiles. Sci Immunol *9*, eadn2362. 10.1126/sciimmunol.adn2362.
15. Garner, L.C., Amini, A., FitzPatrick, M.E.B., Lett, M.J., Hess, G.F., Filipowicz Sinnreich, M., Provine, N.M., and Klenerman, P. (2023). Single-cell analysis of human MAIT cell transcriptional, functional and clonal diversity. Nat Immunol *24*, 1565-1578. 10.1038/s41590-023-01575-1.
16. Mueller, S.N., Gebhardt, T., Carbone, F.R., and Heath, W.R. (2013). Memory T cell subsets, migration patterns, and tissue residence. Annu Rev Immunol *31*, 137-161. 10.1146/annurev-immunol-032712-095954.
17. Maurice, N.J., Taber, A.K., and Prlic, M. (2021). The Ugly Duckling Turned to Swan: A Change in Perception of Bystander-Activated Memory CD8 T Cells. J Immunol *206*, 455-462. 10.4049/jimmunol.2000937.
18. Lee, H., Jeong, S., and Shin, E.C. (2022). Significance of bystander T cell activation in microbial infection. Nat Immunol *23*, 13-22. 10.1038/s41590-021-00985-3.
19. Sekine, T., Perez-Potti, A., Nguyen, S., Gorin, J.B., Wu, V.H., Gostick, E., Llewellyn-Lacey, S., Hammer, Q., Falck-Jones, S., Vangeti, S., et al. (2020). TOX is expressed by exhausted and polyfunctional human effector memory CD8(+) T cells. Sci Immunol *5*. 10.1126/sciimmunol.aba7918.
20. Maurice, N.J., Berner, J., Taber, A.K., Zehn, D., and Prlic, M. (2021). Inflammatory signals are sufficient to elicit TOX expression in mouse and human CD8+ T cells. JCI Insight *6*. 10.1172/jci.insight.150744.
21. Berg, R.E., and Forman, J. (2006). The role of CD8 T cells in innate immunity and in antigen non-specific protection. Curr Opin Immunol *18*, 338-343. 10.1016/j.coi.2006.03.010.
22. Berg, R.E., Cordes, C.J., and Forman, J. (2002). Contribution of CD8+ T cells to innate immunity: IFN-gamma secretion induced by IL-12 and IL-18. Eur J Immunol *32*, 2807-2816. 10.1002/1521-4141(2002010)32:10<2807::AID-IMMU2807>3.0.CO;2-0.
23. Kambayashi, T., Assarsson, E., Lukacher, A.E., Ljunggren, H.G., and Jensen, P.E. (2003). Memory CD8+ T cells provide an early source of IFN-gamma. J Immunol *170*, 2399-2408. 10.4049/jimmunol.170.5.2399.
24. Chu, T., Tyznik, A.J., Roepke, S., Berkley, A.M., Woodward-Davis, A., Pattacini, L., Bevan, M.J., Zehn, D., and Prlic, M. (2013). Bystander-activated memory CD8 T cells control early pathogen load in an innate-like, NKG2D-dependent manner. Cell Rep *3*, 701-708. 10.1016/j.celrep.2013.02.020.
25. Yajima, T., Nishimura, H., Ishimitsu, R., Yamamura, K., Watase, T., Busch, D.H., Pamer, E.G., Kuwano, H., and Yoshikai, Y. (2001). Memory phenotype CD8(+) T cells in IL-15 transgenic mice are involved in early protection against a primary infection with Listeria monocytogenes. Eur J Immunol *31*, 757-766. 10.1002/1521-4141(200103)31:3<757::aid-immu757>3.0.co;2-q.
26. Whiteside, S.K., Snook, J.P., Williams, M.A., and Weis, J.J. (2018). Bystander T Cells: A Balancing Act of Friends and Foes. Trends Immunol *39*, 1021-1035. 10.1016/j.it.2018.10.003.
27. Kim, J., Chang, D.Y., Lee, H.W., Lee, H., Kim, J.H., Sung, P.S., Kim, K.H., Hong, S.H., Kang, W., Lee, J., et al. (2018). Innate-like Cytotoxic Function of Bystander-Activated CD8(+) T Cells Is Associated with Liver Injury in Acute Hepatitis A. Immunity *48*, 161-173 e165. 10.1016/j.immuni.2017.11.025.

822 28. McGeachy, M.J., Cua, D.J., and Gaffen, S.L. (2019). The IL-17 Family of Cytokines in
823 Health and Disease. Immunity *50*, 892-906. 10.1016/j.immuni.2019.03.021.
824 29. Li, J., Casanova, J.L., and Puel, A. (2018). Mucocutaneous IL-17 immunity in mice and
825 humans: host defense vs. excessive inflammation. Mucosal Immunol *11*, 581-589.
826 10.1038/mi.2017.97.
827 30. Sun, L., Su, Y., Jiao, A., Wang, X., and Zhang, B. (2023). T cells in health and disease.
828 Signal Transduct Target Ther *8*, 235. 10.1038/s41392-023-01471-y.
829 31. Singh, N., Baby, D., Rajguru, J.P., Patil, P.B., Thakkannavar, S.S., and Pujari, V.B. (2019).
830 Inflammation and cancer. Ann Afr Med *18*, 121-126. 10.4103/aam.aam_56_18.
831 32. Turner, D.L., and Farber, D.L. (2014). Mucosal resident memory CD4 T cells in protection
832 and immunopathology. Front Immunol *5*, 331. 10.3389/fimmu.2014.00331.
833 33. Arpaia, N., Green, J.A., Moltedo, B., Arvey, A., Hemmers, S., Yuan, S., Treuting, P.M.,
834 and Rudensky, A.Y. (2015). A Distinct Function of Regulatory T Cells in Tissue Protection.
835 Cell *162*, 1078-1089. 10.1016/j.cell.2015.08.021.
836 34. Delacher, M., Schmidleithner, L., Simon, M., Stuve, P., Sanderink, L., Hotz-Wagenblatt,
837 A., Wuttke, M., Schambeck, K., Ruhland, B., Hofmann, V., et al. (2024). The effector
838 program of human CD8 T cells supports tissue remodeling. J Exp Med *221*.
839 10.1084/jem.20230488.
840 35. Konkel, J.E., Cox, J.R., and Wemyss, K. (2024). Bite-sized immunology; damage and
841 microbes educating immunity at the gingiva. Mucosal Immunol *17*, 1141-1150.
842 10.1016/j.mucimm.2024.07.004.
843 36. Kinane, D.F., Stathopoulou, P.G., and Papapanou, P.N. (2017). Periodontal diseases. Nat
844 Rev Dis Primers *3*, 17038. 10.1038/nrdp.2017.38.
845 37. Paprckova, D., Salyova, E., Michalik, J., and Stepanek, O. (2023). Bystander activation in
846 memory and antigen-inexperienced memory-like CD8 T cells. Curr Opin Immunol *82*,
847 102299. 10.1016/j.coi.2023.102299.
848 38. Konecny, A.J., Huang, Y., Setty, M., and Prlic, M. (2024). Signals that control MAIT cell
849 function in healthy and inflamed human tissues. Immunol Rev *323*, 138-149.
850 10.1111/imr.13325.
851 39. Duhen, R., Fesneau, O., Samson, K.A., Frye, A.K., Beymer, M., Rajamanickam, V., Ross,
852 D., Tran, E., Bernard, B., Weinberg, A.D., and Duhen, T. (2022). PD-1 and ICOS
853 coexpression identifies tumor-reactive CD4+ T cells in human solid tumors. J Clin Invest
854 *132*. 10.1172/JCI156821.
855 40. Duhen, T., Duhen, R., Montler, R., Moses, J., Moudgil, T., de Miranda, N.F., Goodall, C.P.,
856 Blair, T.C., Fox, B.A., McDermott, J.E., et al. (2018). Co-expression of CD39 and CD103
857 identifies tumor-reactive CD8 T cells in human solid tumors. Nat Commun *9*, 2724.
858 10.1038/s41467-018-05072-0.
859 41. Simoni, Y., Becht, E., Fehlings, M., Loh, C.Y., Koo, S.L., Teng, K.W.W., Yeong, J.P.S.,
860 Nahar, R., Zhang, T., Kared, H., et al. (2018). Bystander CD8(+) T cells are abundant and
861 phenotypically distinct in human tumour infiltrates. Nature *557*, 575-579. 10.1038/s41586-
862 018-0130-2.
863 42. de Goffau, M.C., Lager, S., Sovio, U., Gaccioli, F., Cook, E., Peacock, S.J., Parkhill, J.,
864 Charnock-Jones, D.S., and Smith, G.C.S. (2019). Human placenta has no microbiome but
865 can contain potential pathogens. Nature *572*, 329-334. 10.1038/s41586-019-1451-5.
866 43. Briana, D.D., Papaevangelou, V., and Malamitsi-Puchner, A. (2021). The jury is still out
867 on the existence of a placental microbiome. Acta Paediatr *110*, 2958-2963.
868 10.1111/apa.16048.
869 44. Whiteside, S.A., McGinniss, J.E., and Collman, R.G. (2021). The lung microbiome:
870 progress and promise. J Clin Invest *131*. 10.1172/JCI150473.
871 45. Maher, T.M. (2024). Interstitial Lung Disease: A Review. JAMA *331*, 1655-1665.
872 10.1001/jama.2024.3669.

46. Jung, E., Romero, R., Suksai, M., Gotsch, F., Chaemsaithong, P., Erez, O., Conde-Agudelo, A., Gomez-Lopez, N., Berry, S.M., Meyyazhagan, A., and Yoon, B.H. (2024). Clinical chorioamnionitis at term: definition, pathogenesis, microbiology, diagnosis, and treatment. Am J Obstet Gynecol *230*, S807-S840. 10.1016/j.ajog.2023.02.002.
47. Sakuishi, K., Ngiow, S.F., Sullivan, J.M., Teng, M.W., Kuchroo, V.K., Smyth, M.J., and Anderson, A.C. (2013). TIM3(+)FOXP3(+) regulatory T cells are tissue-specific promoters of T-cell dysfunction in cancer. Oncoimmunology *2*, e23849. 10.4161/onci.23849.
48. Voo, K.S., Wang, Y.H., Santori, F.R., Boggiano, C., Wang, Y.H., Arima, K., Bover, L., Hanabuchi, S., Khalili, J., Marinova, E., et al. (2009). Identification of IL-17-producing FOXP3+ regulatory T cells in humans. Proc Natl Acad Sci U S A *106*, 4793-4798. 10.1073/pnas.0900408106.
49. Beriou, G., Costantino, C.M., Ashley, C.W., Yang, L., Kuchroo, V.K., Baecher-Allan, C., and Hafler, D.A. (2009). IL-17-producing human peripheral regulatory T cells retain suppressive function. Blood *113*, 4240-4249. 10.1182/blood-2008-10-183251.
50. Dominguez-Villar, M., Baecher-Allan, C.M., and Hafler, D.A. (2011). Identification of T helper type 1-like, Foxp3+ regulatory T cells in human autoimmune disease. Nat Med *17*, 673-675. 10.1038/nm.2389.
51. Wang, J., Ioan-Facsinay, A., van der Voort, E.I., Huizinga, T.W., and Toes, R.E. (2007). Transient expression of FOXP3 in human activated nonregulatory CD4+ T cells. Eur J Immunol *37*, 129-138. 10.1002/eji.200636435.
52. Galant-Swafford, J., Catanzaro, J., Achcar, R.D., Cool, C., Koelsch, T., Bang, T.J., Lynch, D.A., Alam, R., Katial, R.K., and Fernandez Perez, E.R. (2024). Approach to diagnosing and managing granulomatous-lymphocytic interstitial lung disease. EClinicalMedicine *75*, 102749. 10.1016/j.eclinm.2024.102749.
53. Cao, S., Liu, X., Li, Y., Yang, Y., Cai, X., Cong, S., Li, Z., Li, Y., Hong, Y., Su, Y., et al. (2024). Serum sCD25 is an indicator for rheumatoid arthritis-associated interstitial lung disease. Clin Exp Rheumatol *42*, 633-641. 10.55563/clinexprheumatol/3iqvk3.
54. Chen, H., Tang, J., Liang, J., Huang, D., Pan, C., Liu, S., Du, X., and Tao, L. (2023). Clinical association study on the matrix metalloproteinase expression in the serum of patients with connective tissue disease complicated with interstitial lung disease. Arch Rheumatol *38*, 367-374. 10.46497/ArchRheumatol.2023.9547.
55. Sheu, B.C., Hsu, S.M., Ho, H.N., Lien, H.C., Huang, S.C., and Lin, R.H. (2001). A novel role of metalloproteinase in cancer-mediated immunosuppression. Cancer Res *61*, 237-242.
56. Kim, T.S., Silva, L.M., Theofilou, V.I., Greenwell-Wild, T., Li, L., Williams, D.W., Ikeuchi, T., Brenchley, L., Genomics, N.N., Computational Biology, C., et al. (2023). Neutrophil extracellular traps and extracellular histones potentiate IL-17 inflammation in periodontitis. J Exp Med *220*. 10.1084/jem.20221751.
57. Dutzan, N., Kajikawa, T., Abusleme, L., Greenwell-Wild, T., Zuazo, C.E., Ikeuchi, T., Brenchley, L., Abe, T., Hurabielle, C., Martin, D., et al. (2018). A dysbiotic microbiome triggers T(H)17 cells to mediate oral mucosal immunopathology in mice and humans. Sci Transl Med *10*. 10.1126/scitranslmed.aat0797.
58. Woodward Davis, A.S., Roozen, H.N., Dufort, M.J., DeBerg, H.A., Delaney, M.A., Mair, F., Erickson, J.R., Slichter, C.K., Berkson, J.D., Klock, A.M., et al. (2019). The human tissue-resident CCR5(+) T cell compartment maintains protective and functional properties during inflammation. Sci Transl Med *11*. 10.1126/scitranslmed.aaw8718.
59. Zielinski, C.E., Mele, F., Aschenbrenner, D., Jarrossay, D., Ronchi, F., Gattorno, M., Monticelli, S., Lanzavecchia, A., and Sallusto, F. (2012). Pathogen-induced human TH17 cells produce IFN-gamma or IL-10 and are regulated by IL-1beta. Nature *484*, 514-518. 10.1038/nature10957.

60. Ginesin, O., Coyac, B.R., Doppelt-Flikshtain, O., Mayer, Y., Gabay, E., Berg, T., Bar-On, Y., and Zigdon-Giladi, H. (2025). Macrophage Depletion Reduces Bone Loss and Alters Inflammatory Responses: A Mouse Peri-Implantitis Model. J Clin Periodontol *52*, 898-906. 10.1111/jcpe.14120.
61. Moutsopoulos, N.M., Konkel, J., Sarmadi, M., Eskan, M.A., Wild, T., Dutzan, N., Abusleme, L., Zenobia, C., Hosur, K.B., Abe, T., et al. (2014). Defective neutrophil recruitment in leukocyte adhesion deficiency type I disease causes local IL-17-driven inflammatory bone loss. Sci Transl Med *6*, 229ra240. 10.1126/scitranslmed.3007696.
62. Misharin, A.V., Morales-Nebreda, L., Reyfman, P.A., Cuda, C.M., Walter, J.M., McQuattie-Pimentel, A.C., Chen, C.I., Anekalla, K.R., Joshi, N., Williams, K.J.N., et al. (2017). Monocyte-derived alveolar macrophages drive lung fibrosis and persist in the lung over the life span. J Exp Med *214*, 2387-2404. 10.1084/jem.20162152.
63. Prasse, A., Pechkovsky, D.V., Toews, G.B., Jungraithmayr, W., Kollert, F., Goldmann, T., Vollmer, E., Muller-Quernheim, J., and Zissel, G. (2006). A vicious circle of alveolar macrophages and fibroblasts perpetuates pulmonary fibrosis via CCL18. Am J Respir Crit Care Med *173*, 781-792. 10.1164/rccm.200509-1518OC.
64. Zhang, C., Cao, J., Xu, M., Wu, D., Li, W., and Chang, Y. (2023). The role of neutrophils in chorioamnionitis. Front Immunol *14*, 1198831. 10.3389/fimmu.2023.1198831.
65. Leelatian, N., Doxie, D.B., Greenplate, A.R., Mobley, B.C., Lehman, J.M., Sinnaeve, J., Kauffmann, R.M., Werkhaven, J.A., Mistry, A.M., Weaver, K.D., et al. (2017). Single cell analysis of human tissues and solid tumors with mass cytometry. Cytometry B Clin Cytom *92*, 68-78. 10.1002/cyto.b.21481.
66. Maurice, N.J., Erickson, J.R., DeJong, C.S., Mair, F., Taber, A.K., Frutoso, M., Islas, L.V., Vigil, A., Lawler, R.L., McElrath, J., et al. (2025). Cytokine and metabolite networks shape T cell residency and functionality at the term human maternal-fetal interface. J Immunol *214*, 2221-2237. 10.1093/jimmun/vkaf093.
67. Mair, F., Erickson, J.R., Frutoso, M., Konecny, A.J., Greene, E., Voillet, V., Maurice, N.J., Rongvaux, A., Dixon, D., Barber, B., et al. (2022). Extricating human tumour immune alterations from tissue inflammation. Nature *605*, 728-735. 10.1038/s41586-022-04718-w.
68. Mair, F., and Tyznik, A.J. (2019). High-Dimensional Immunophenotyping with Fluorescence-Based Cytometry: A Practical Guidebook. Methods Mol Biol *2032*, 1-29. 10.1007/978-1-4939-9650-6_1.
69. Ashhurst, T.M., Marsh-Wakefield, F., Putri, G.H., Spiteri, A.G., Shinko, D., Read, M.N., Smith, A.L., and King, N.J.C. (2022). Integration, exploration, and analysis of high-dimensional single-cell cytometry data using Spectre. Cytometry A *101*, 237-253. 10.1002/cyto.a.24350.
70. Putri, G.H., Howitt, G., Marsh-Wakefield, F., Ashhurst, T.M., and Phipson, B. (2024). SuperCellCyto: enabling efficient analysis of large scale cytometry datasets. Genome Biol *25*, 89. 10.1186/s13059-024-03229-3.
71. Bilous, M., Herault, L., Gabriel, A.A., Teleman, M., and Gfeller, D. (2024). Building and analyzing metacells in single-cell genomics data. Mol Syst Biol *20*, 744-766. 10.1038/s44320-024-00045-6.
72. Liu, X., Song, W., Wong, B.Y., Zhang, T., Yu, S., Lin, G.N., and Ding, X. (2019). A comparison framework and guideline of clustering methods for mass cytometry data. Genome Biol *20*, 297. 10.1186/s13059-019-1917-7.
73. Traag, V.A., Waltman, L., and van Eck, N.J. (2019). From Louvain to Leiden: guaranteeing well-connected communities. Sci Rep *9*, 5233. 10.1038/s41598-019-41695-z.
74. Levine, J.H., Simonds, E.F., Bendall, S.C., Davis, K.L., Amir el, A.D., Tadmor, M.D., Litvin, O., Fienberg, H.G., Jager, A., Zunder, E.R., et al. (2015). Data-Driven Phenotypic

973 Dissection of AML Reveals Progenitor-like Cells that Correlate with Prognosis. Cell *162*,
974 184-197. 10.1016/j.cell.2015.05.047.
975 75. Becht, E., McInnes, L., Healy, J., Dutertre, C.A., Kwok, I.W.H., Ng, L.G., Ginhoux, F., and
976 Newell, E.W. (2018). Dimensionality reduction for visualizing single-cell data using UMAP.
977 Nat Biotechnol. 10.1038/nbt.4314.

978

Figure 1

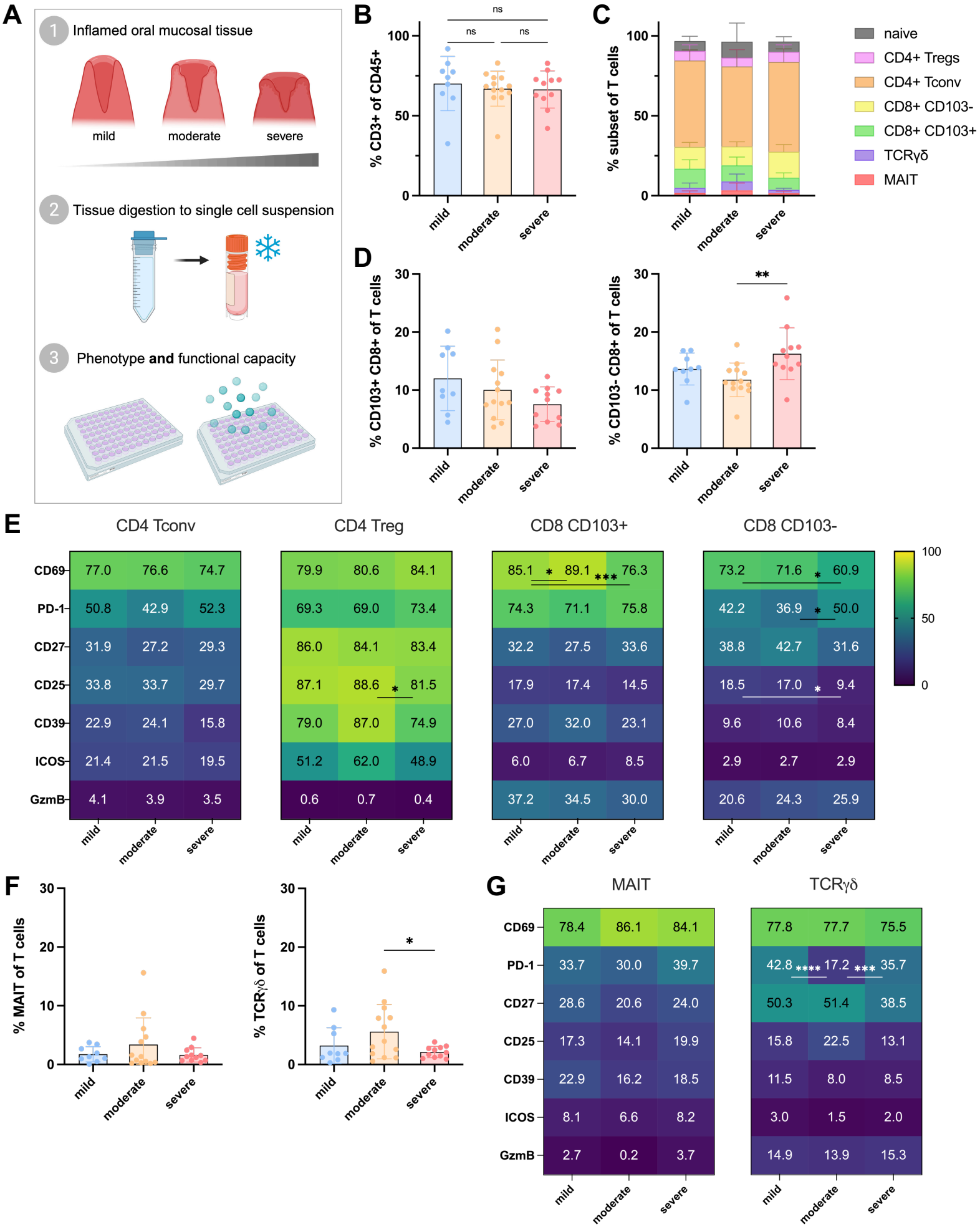
A
1 Inflamed oral mucosal tissue
mild
moderate
severe
2 Tissue digestion to single cell suspension
3 Phenotype and functional capacity
B
% CD3+ of CD45+
ns
ns
ns
mild
moderate
severe
C
% subset of T cells
naive
CD4+ Tregs
CD4+ Tconv
CD8+ CD103-
CD8+ CD103+
TCRγδ
MAIT
D
% CD103+ CD8+ of T cells
% CD103- CD8+ of T cells
**
E
CD4 Tconv
CD4 Treg
CD8 CD103+
CD8 CD103-
CD69
PD-1
CD27
CD25
CD39
ICOS
GzmB
F
% MAIT of T cells
% TCRγδ of T cells
*
G
MAIT
TCRγδ
****
***

Figure 2

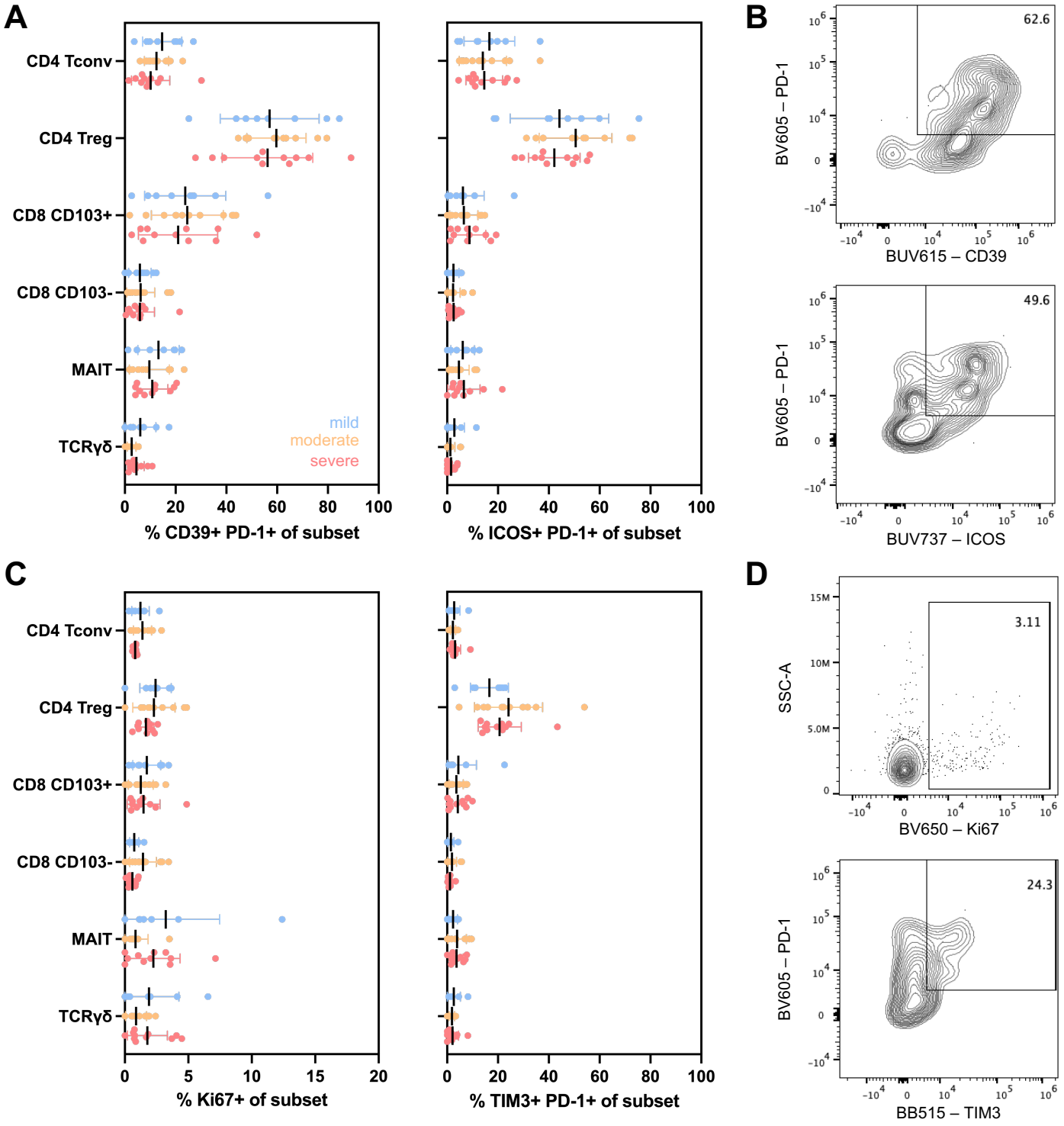
A
CD4 Tconv
CD4 Treg
CD8 CD103+
CD8 CD103-
MAIT
TCRγδ
mild
moderate
severe
% CD39+ PD-1+ of subset
% ICOS+ PD-1+ of subset
B
62.6
BV605 – PD-1
BUV615 – CD39
49.6
BV605 – PD-1
BUV737 – ICOS
C
% Ki67+ of subset
% TIM3+ PD-1+ of subset
D
3.11
SSC-A
BV650 – Ki67
24.3
BV605 – PD-1
BB515 – TIM3

Figure 3

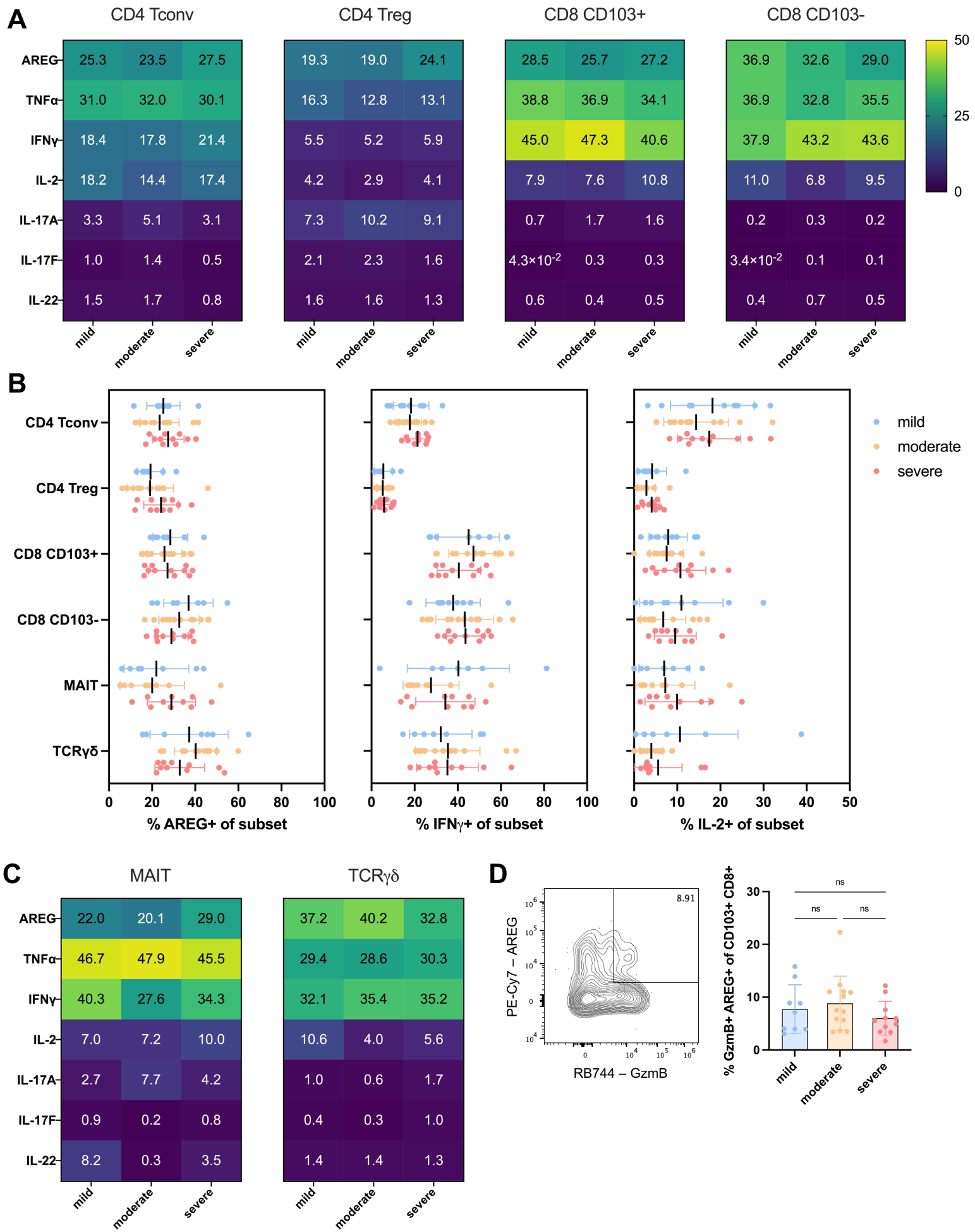
A
CD4 Tconv
CD4 Treg
CD8 CD103+
CD8 CD103-
AREG
TNFα
IFNγ
IL-2
IL-17A
IL-17F
IL-22
mild
moderate
severe
B
CD4 Tconv
CD4 Treg
CD8 CD103+
CD8 CD103-
MAIT
TCRγδ
% AREG+ of subset
% IFNγ+ of subset
% IL-2+ of subset
mild
moderate
severe
C
MAIT
TCRγδ
D
PE-Cy7 – AREG
RB744 – GzmB
8.91
% GzmB+ AREG+ of CD103+ CD8+
ns

Figure 4

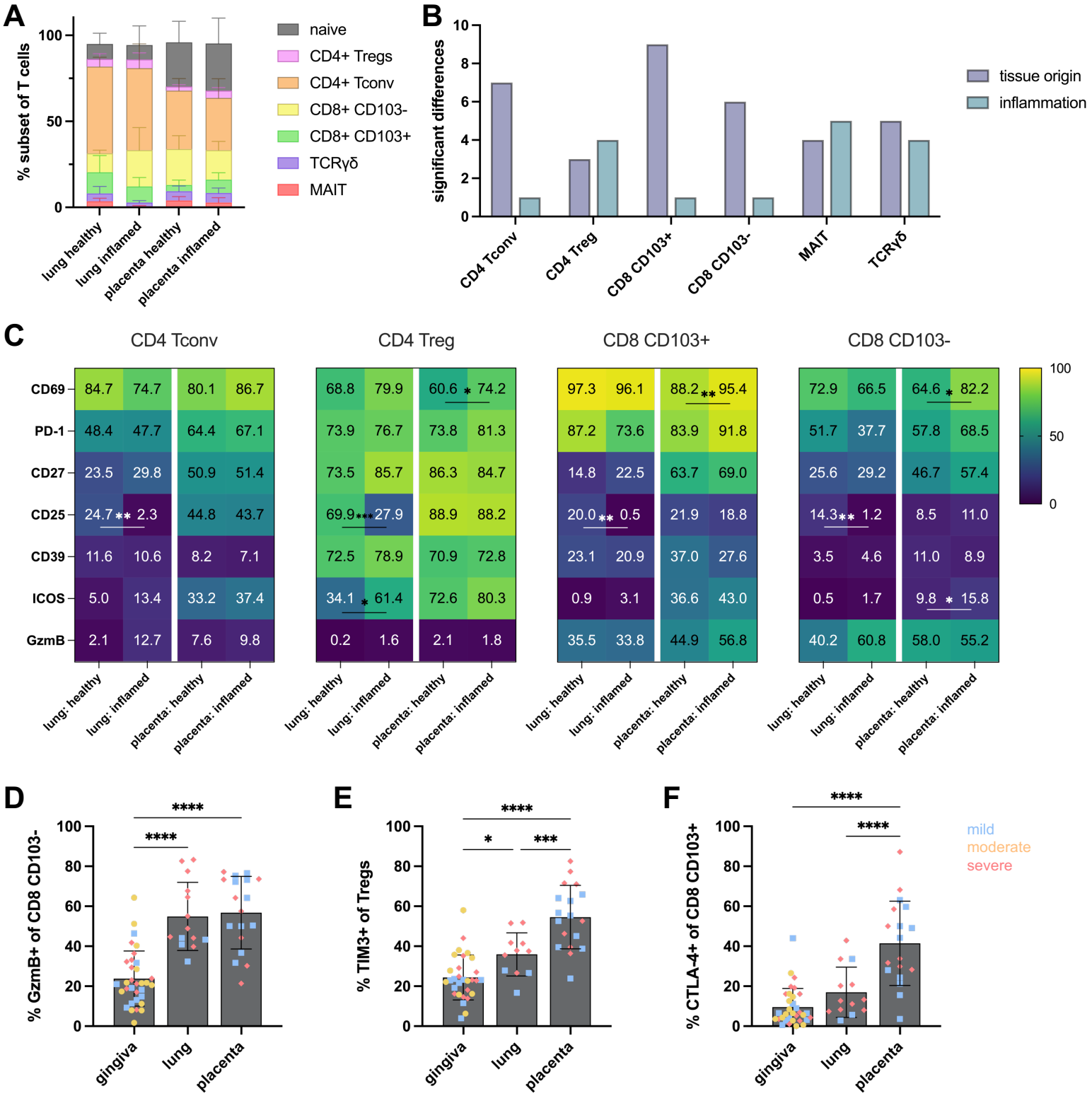
A
% subset of T cells
100
50
0
lung healthy
lung inflamed
placenta healthy
placenta inflamed
naive
CD4+ Tregs
CD4+ Tconv
CD8+ CD103-
CD8+ CD103+
TCRγδ
MAIT
B
significant differences
10
8
6
4
2
0
CD4 Tconv
CD4 Treg
CD8 CD103+
CD8 CD103-
MAIT
TCRγδ
tissue origin
inflammation
C
CD4 Tconv
CD4 Treg
CD8 CD103+
CD8 CD103-
CD69
PD-1
CD27
CD25
CD39
ICOS
GzmB
84.7 74.7 80.1 86.7
48.4 47.7 64.4 67.1
23.5 29.8 50.9 51.4
24.7 ** 2.3 44.8 43.7
11.6 10.6 8.2 7.1
5.0 13.4 33.2 37.4
2.1 12.7 7.6 9.8
68.8 79.9 60.6 * 74.2
73.9 76.7 73.8 81.3
73.5 85.7 86.3 84.7
69.9 *** 27.9 88.9 88.2
72.5 78.9 70.9 72.8
34.1 * 61.4 72.6 80.3
0.2 1.6 2.1 1.8
97.3 96.1 88.2 ** 95.4
87.2 73.6 83.9 91.8
14.8 22.5 63.7 69.0
20.0 ** 0.5 21.9 18.8
23.1 20.9 37.0 27.6
0.9 3.1 36.6 43.0
35.5 33.8 44.9 56.8
72.9 66.5 64.6 * 82.2
51.7 37.7 57.8 68.5
25.6 29.2 46.7 57.4
14.3 ** 1.2 8.5 11.0
3.5 4.6 11.0 8.9
0.5 1.7 9.8 * 15.8
40.2 60.8 58.0 55.2
lung: healthy
lung: inflamed
placenta: healthy
placenta: inflamed
100
50
0
D
% GzmB+ of CD8 CD103-
****
****
gingiva
lung
placenta
E
% TIM3+ of Tregs
****
*
***
gingiva
lung
placenta
F
% CTLA-4+ of CD8 CD103+
****
****
gingiva
lung
placenta
mild
moderate
severe

Figure 5

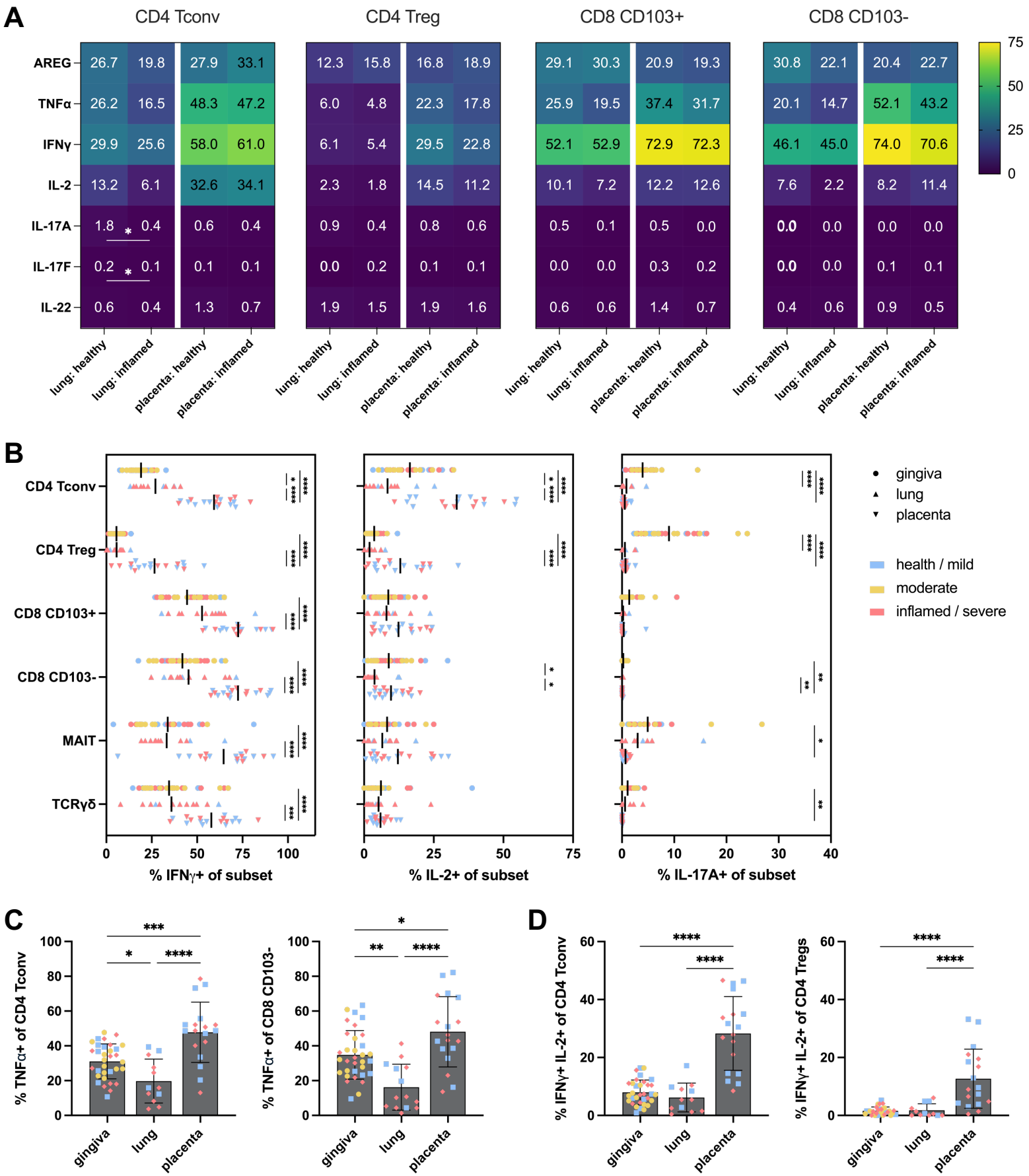
A
CD4 Tconv
CD4 Treg
CD8 CD103+
CD8 CD103-
AREG
TNFα
IFNγ
IL-2
IL-17A
IL-17F
IL-22
lung: healthy
lung: inflamed
placenta: healthy
placenta: inflamed
B
CD4 Tconv
CD4 Treg
CD8 CD103+
CD8 CD103-
MAIT
TCRγδ
% IFNγ+ of subset
% IL-2+ of subset
% IL-17A+ of subset
gingiva
lung
placenta
health / mild
moderate
inflamed / severe
C
% TNFα+ of CD4 Tconv
% TNFα+ of CD8 CD103-
D
% IFNγ+ IL-2+ of CD4 Tconv
% IFNγ+ IL-2+ of CD4 Tregs

Figure 6

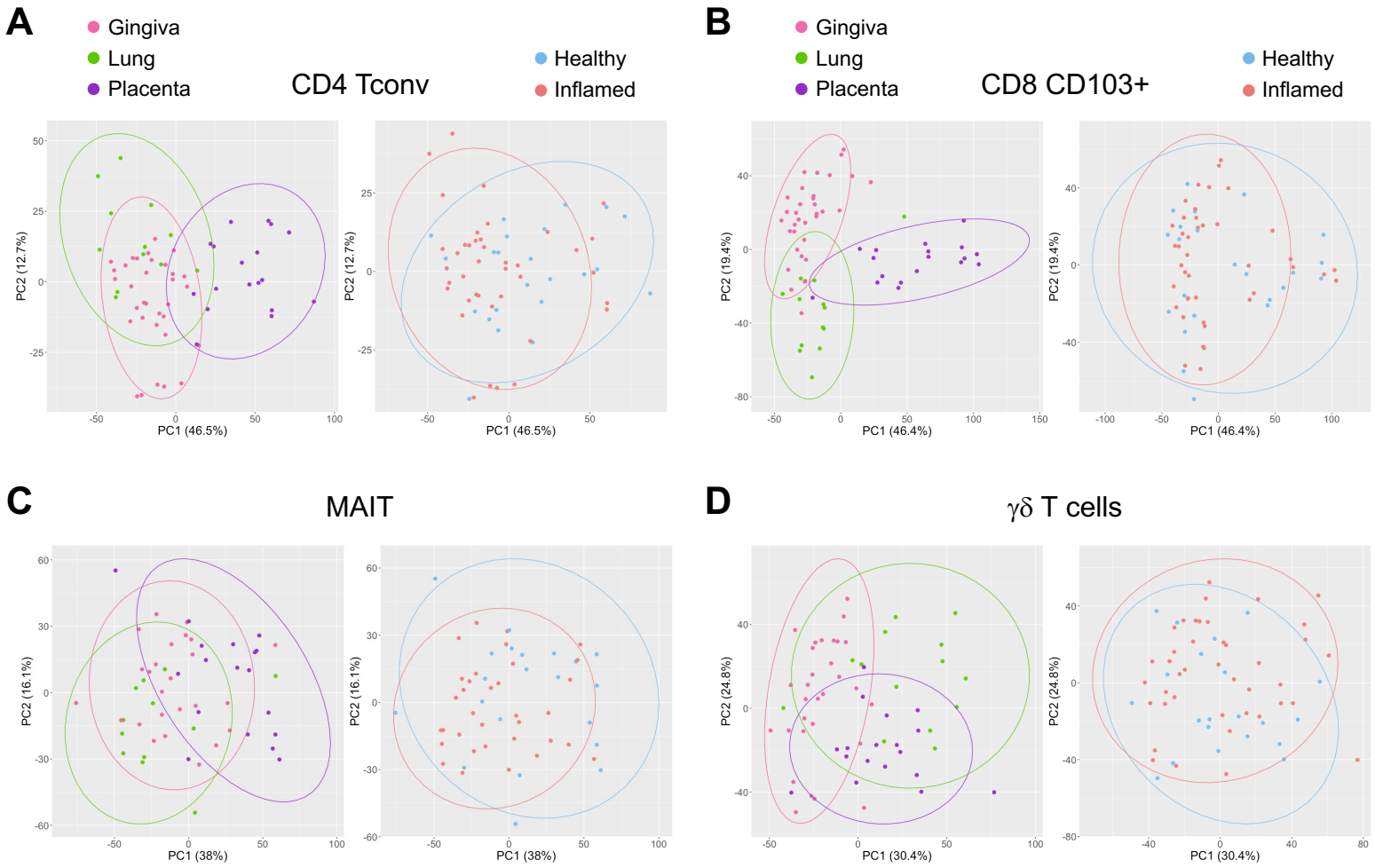
A
Gingiva
Lung
Placenta
CD4 Tconv
Healthy
Inflamed
PC2 (12.7%)
PC1 (46.5%)
B
Gingiva
Lung
Placenta
CD8 CD103+
Healthy
Inflamed
PC2 (19.4%)
PC1 (46.4%)
C
MAIT
PC2 (16.1%)
PC1 (38%)
D
γδ T cells
PC2 (24.8%)
PC1 (30.4%)

Figure 7

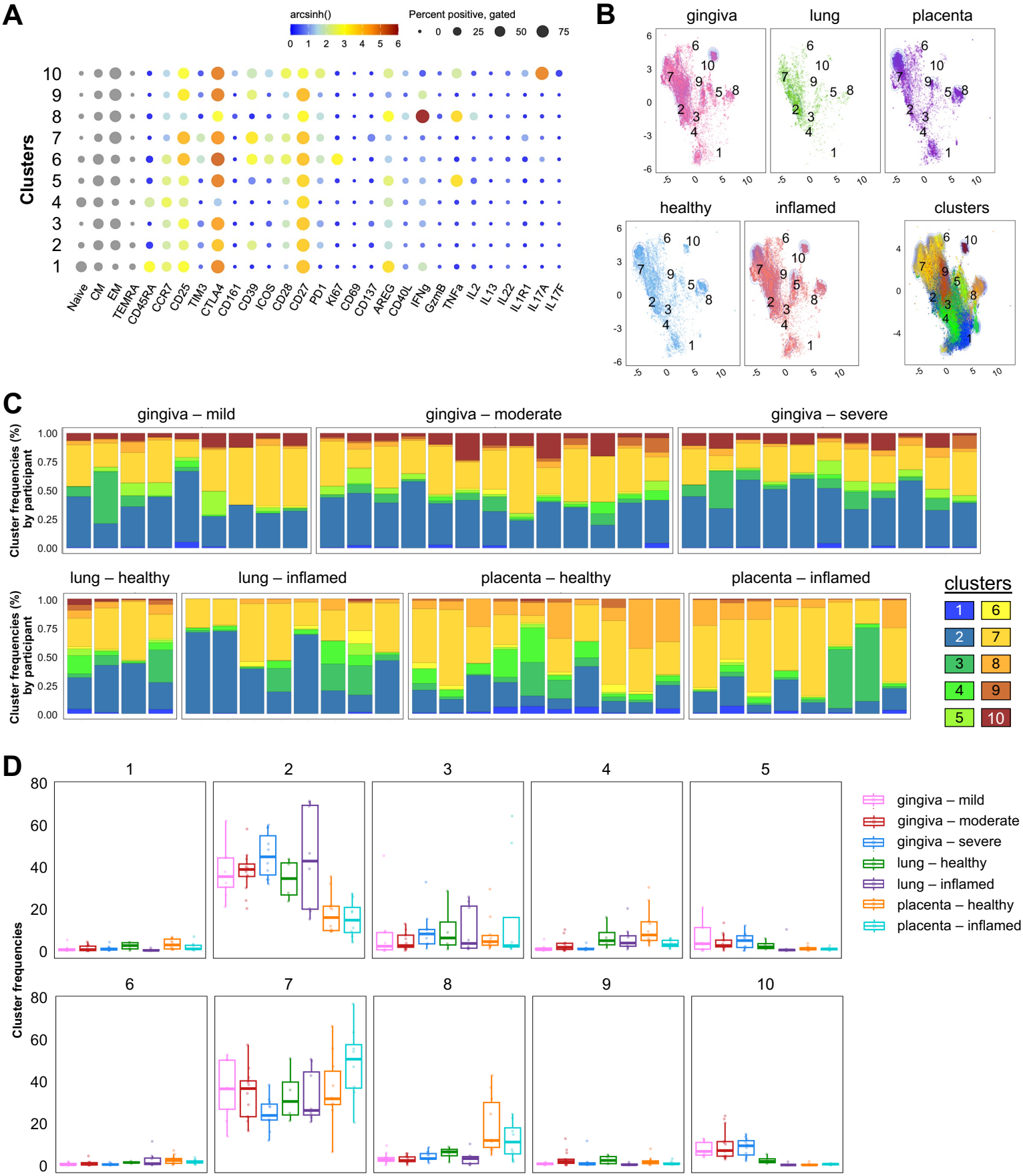
A
arcsinh()
Percent positive, gated
Clusters
Naive
CM
EM
TEMRA
CD45RA
CCR7
CD25
TIM3
CTLA4
CD161
CD39
ICOS
CD28
CD27
PD1
Ki67
CD69
CD137
AREG
CD40L
IFNg
GzmB
TNFa
IL2
IL13
IL22
IL1R1
IL17A
IL17F
B
gingiva
lung
placenta
healthy
inflamed
clusters
C
gingiva – mild
gingiva – moderate
gingiva – severe
lung – healthy
lung – inflamed
placenta – healthy
placenta – inflamed
Cluster frequencies (%) by participant
clusters
D
Cluster frequencies
gingiva – mild
gingiva – moderate
gingiva – severe
lung – healthy
lung – inflamed
placenta – healthy
placenta – inflamed